Chem Soc Rev

REVIEW ARTICLE

View Article Online
View Journal | View Issue

New materials for tunable plasmonic colloidal nanocrystals

Cite this: *Chem. Soc. Rev.*, 2014, **43**, 3957

Alberto Comin*[ab] and Liberato Manna*[bc]

Received 20th July 2013

DOI: 10.1039/c3cs60265f

www.rsc.org/csr

We present a review on the emerging materials for novel plasmonic colloidal nanocrystals. We start by explaining the basic processes involved in surface plasmon resonances in nanoparticles and then discuss the classes of nanocrystals that to date are particularly promising for tunable plasmonics: non-stoichiometric copper chalcogenides, extrinsically doped metal oxides, oxygen-deficient metal oxides and conductive metal oxides. We additionally introduce other emerging types of plasmonic nanocrystals and finally we give an outlook on nanocrystals of materials that could potentially display interesting plasmonic properties.

Introduction

Plasmonic nanocrystals (NCs) are a versatile class of nanoparticles that are finding application in several fields:[1–9] they have been proposed for example as chemical probes due to the high sensitivity of their optical response to their immediate surrounding environment,[3,6,7] as heat mediators in hyperthermia therapy,[4,8,9] and as light concentrators in solar cells.[4,5] Their properties stem from the possibility to induce in them collective oscillations of free charge carriers.[1] These excitations are related to the surface plasmon resonances (SPRs), which are typical of bulk metals and which in nanoparticles are called "localized SPRs" (LSPRs).[1] LSPRs appear only in objects which are much smaller than the wavelength of the incident light. Indeed, thanks to the reduced size, all free carriers can oscillate in phase with the external electric filed,[1] and the antenna effect,[10] caused by their coherent motions, provides the strong electric field enhancement that is commonly associated with plasmonic NCs.[4]

The number of possible materials that can sustain a LSPR is virtually infinite, since there are many possible ways to achieve a population of free carriers in a nanosized material. Only

[a] *Ludwig-Maximilians-Universtität, Butenandtstrasse 5–13 E, 81377 München, Germany. E-mail: alberto.comin@cup.uni-muenchen.de; Fax: +49 892180 77601; Tel: +49 892180 77188*

[b] *Istituto Italiano di Tecnologia, via Morego 30, 16163 Genova, Italy. E-mail: liberato.manna@iit.it; Fax: +39 01071781*

[c] *Kavli Institute of NanoScience, Delft University of Technology, Lorentzweg 1, 2628 CJ Delft, The Netherlands*

Alberto Comin

Alberto Comin studied physics at the University of Pavia, Italy. He received his PhD in 2004 from the University of Milan, Italy, with a thesis on ultrafast spin dynamics in transition metal films. He worked for three years at the Lawrence Berkeley National Laboratory doing research on ultrafast magnetization dynamics studied by time-resolved X-ray spectroscopy. He then moved back to Italy as a researcher at the Italian Institute of Technology. His research focuses on the understanding of the carrier and spin dynamics in plasmonic and magnetic nanostructures, studied with femtosecond temporal resolution. He is currently at the Ludwig Maximilians Universität München.

Liberato Manna

Liberato Manna received his PhD in Chemistry in 2001 from the University of Bari (Italy) and worked at the University of California Berkeley as visiting student and then at the Lawrence Berkeley Lab as postdoc until 2003. He was then scientist at the National Nanotechnology Lab in Lecce (Italy) and in 2009 he moved to the Istituto Italiano di Tecnologia, Genova (Italy) as director of the Nanochemistry Department. Since 2010 he is also part-time professor at TU Delft (The Netherlands). His research interests are the synthesis and assembly of inorganic nanostructures for applications in various fields and the study of structural and chemical transformations in nanocrystals.

recently, though, *via* the development of semiconductor-based NCs, it has been possible to get more control of the LSPR, for instance by the acquired ability to shift it reversibly to lower or higher energies or by dynamically switching it by a laser pulse or by applying a static electric field. NCs of metals like Au, Ag and Cu are easiest to synthesize and, in the case of Au, they are stable against oxidation. Also, their LSPRs are in a range of energies suitable for several applications, in contrast to that of most metals for which LSPRs are in the deep ultraviolet region (>8 eV). Therefore they have been the subject of intensive investigation in the last few years.[11] However, these are not ideal plasmonic materials, one major issue being their high optical losses, that is, losses due to electronic transitions. They are not even ideal for fabricating meta-materials and transformation-optics devices, due to a large real component of their dielectric constant. Since the real component of the permittivity for dielectric materials is generally much smaller than in metals, this poses fabrication issues related to the fact that the metal components have to be much smaller than the dielectric ones. On the other hand, new types of plasmonic materials and, in parallel to that, new types of plasmonic NCs have emerged recently.[12] The vast majority of "alternative" plasmonic NCs to date can be grouped into the following classes:

(i) NCs of extrinsically doped "traditional" semiconductors and metal oxides, in which extra carriers are generally provided by the dopant atoms. In extrinsically doped NCs, the number of free carriers is of the same order as the number of impurities/defects but generally lower than that, since a portion of the extra carriers can be trapped or may not have enough mobility to contribute to the plasmonic band. For these materials tuning is generally achieved during their synthesis or even *via* post-synthesis treatments,[13] for example by direct injection of electrical carriers.[14]

(ii) NCs of copper deficient copper chalcogenides and of oxygen deficient metal oxides, also called "self-doped materials". In self-doped materials, free carriers arise from the variation in the oxidation state of generally one of their elements in non-stoichiometric phases. This is required in order to compensate for the sub-stoichiometry of one of the components, and results either in extra electrons in the conduction band, or in holes in an otherwise filled valence band. For these NCs, "self-doping" can be also achieved *via* post-synthetic redox processes.[15]

(iii) NCs of metal oxides that, due to their intrinsic electronic structure, have conductive behaviour.

In the first two classes of materials, the carrier concentration can be varied in order to tune the SPR frequency across the visible and infrared range.[16] This is not possible in metals such as Au, Ag or Cu, for which the carrier density stays fixed.[1] In principle, these novel plasmonic NCs can complement and perhaps supplant metals in many nanophotonics applications,[17] in particular those that require modulating or switching on and off the plasmonic properties.[14] Most of these plasmonic NCs have LSPRs in the near infrared (NIR) region of the spectrum, which makes them promising for imaging of biological tissues and for hyperthermia therapy, because the penetration depth of light increases significantly towards the infrared.[18] These novel types of NCs could also be used for solar cells which harvest the infrared portion of the solar spectrum, or in smart windows that transmit or block visible light and heat, therefore improving the energy efficiency of buildings.[14] The reversible tunability of the LSPRs is arguably one of the strongest points in favour of semiconductor NCs, as compared to metals. This could be exploited for realising waveguide modulators and switches at telecommunication wavelengths.[14,19]

In this review, we will first give a brief introduction on the nature of LSPRs and on the basic physics involved. Then we will describe the various classes of emergent plasmonic NCs that are currently under intense investigation and will highlight the proposed applications. Finally, we will give an outlook on NCs of additional materials that could potentially display useful plasmonic properties.

A brief introduction to plasmonic NCs

The Drude model

In order to better describe the LSPRs in NCs, we need to introduce some general concepts related to the optical response in metals. We begin with the Drude model of the dielectric permittivity of metals, which is described by the formula[1]

$$\varepsilon = \varepsilon_\infty - \omega_p{}^2/(\omega^2 + i\gamma\omega) \quad (1)$$

The model assumes that the collective motion of the free electrons determines the optical response, *via* the plasma frequency ω_p, the damping parameter γ and a background dielectric constant ε_∞, due to interband transitions at higher frequencies. The plasma frequency is defined as[20]

$$\omega_p{}^2 = \frac{n_e e^2}{\varepsilon_0 m^*} \quad (2)$$

where n_e is the free carrier density and m^* is their effective mass. We note that the previous expression was originally written for metals but it is also generally valid for any material in which free carriers are present, for example doped semiconductors. In the model, the damping parameter γ is purely classical and represents the frequency of carrier scattering events.[20] This is defined as $\gamma = e/(\mu m^*)$, where μ is the carrier mobility. For a NC of a few nm in diameter, this damping parameter is bigger than for the corresponding bulk material, because the size of the NC is comparable to the mean free path of the carriers. In this circumstance the scattering of carriers with the surface of the NC becomes relevant and, to account for this effect, γ can be rewritten as

$$\gamma = \gamma_b + A\nu_F/D \quad (3)$$

In the above expression, γ_b is the damping parameter in the bulk, ν_F is the Fermi velocity and D is the diameter of the NC. This model has a simple physical interpretation, since ν_F/D is the time that is required for a classic particle to travel from one side to the opposite side of the NC. The surface scattering is also responsible for a slight shift of the LSPR resonance, when the NC size decreases below about 3 nm, a trend which has

been observed both in metal NCs (see ref. 21 and references therein) and in copper chalcogenide NCs.[22]

Conditions for observing LSPR in NCs

LSPRs are generally observed in metal NCs of sizes greater than a couple of nanometers and smaller than one-fifth of the LSPR wavelength.[1] Within this range, the electronic structure of the particle is similar to that of the corresponding bulk material, and the dielectric polarization can be considered as uniform inside each NC. It is therefore possible to neglect the cross-terms of the Maxwell equations, which couple electric and magnetic fields. Under this approximation, the laws of electrostatics well describe the coherent response of the free electrons. Usually for very small NCs the optical response is dominated by the dipole contribution, given by the formula[4]

$$\alpha = 4\pi R^3 \frac{\varepsilon - \varepsilon_m}{\varepsilon + 2\varepsilon_m} \quad (4)$$

which expresses the electric polarization α of a NC of radius R, as a function of the dielectric permittivities of the NC (ε) and of the embedding medium (ε_m). To better understand the conditions under which a LSPR can be observed in a metal NC, let us rewrite the Drude permittivity of a metal of eqn (1) as the sum of the real and the imaginary components

$$\varepsilon(\omega) = \varepsilon' + i\varepsilon'' = \varepsilon_\infty - \frac{\omega_p^2}{\omega^2 + \gamma^2} + i\frac{\omega_p^2 \gamma}{\omega(\omega^2 + \gamma^2)} \quad (5)$$

Fig. 1a reports for example the real part of the permittivity of gold,[23] as a function of the photon energy. Assuming that for both the metal and the dielectric in the region of interest the imaginary components of their permittivities are negligible (see later), the LSPR energy is given by the condition $\varepsilon'(\omega) = -2\varepsilon_m$. This can be graphically determined as the intersection of the permittivity curve with the horizontal line drawn at $-2\varepsilon_m$, as illustrated in Fig. 1a. It can be seen that the LSPR energy decreases as the permittivity of the medium increases. By this simple model one can appreciate why LSPRs are very sensitive to changes in the local environment. Fig. 1b shows the absorption spectra of gold NCs embedded in different dielectric environments, calculated in the dipole approximation (eqn (4)) and using published data for the permittivity of gold.[23] In the same figure, it can be noted that the central frequencies of the LSPRs are slightly shifted with respect to the predicted value, by the effect of the imaginary part of the permittivity of gold.

The same conditions that we have just illustrated, by referring to gold as a model, apply to NCs of any material in which free carriers are present, for example a doped semiconductor, if in that range of frequencies the material behaves indeed as a metal (see below). The main difference of a doped semiconductor with respect to a metal (like gold or silver) is that, due to the reduced density of free carriers in the doped semiconductor, its LSPR energy will be lower than that of a metal like gold or silver. As for the metal, since the electric field extends beyond the geometrical boundary of the nanoparticles, the spectral position of the LSPR in the NC of a doped semiconductor depends on the dielectric permittivity of the surrounding material.[24] The condition

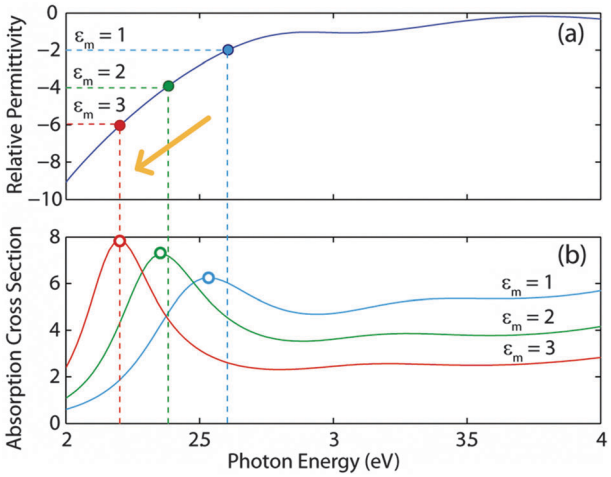

Fig. 1 Dependence of the LSPR frequency of gold NCs on the dielectric permittivity of the surrounding environment. (a) The resonance condition can be graphically visualized by intersecting the real part of the permittivity of gold with a horizontal line drawn at −2 times the permittivity of the environment; (b) the absorption spectra of Au NCs, calculated in the dipole approximation for different environments, show that the LSPR is shifted to lower frequencies as the permittivity of the environment is increased. The slight mismatch between the two panels is due to the imaginary part of the permittivity of gold, which is not taken into account in the graphic model.

for a material to exhibit metallic behaviour in its optical properties is for the real component of its permittivity to be negative ($\varepsilon' < 0$). Since free carriers contribute with a term that decreases in the direction of lower photon energies (see eqn (5)), for all conductive materials there is a cross-over frequency ω_c (at which $\varepsilon' = 0$) below which the real part of the permittivity becomes negative.

The cross-over frequency depends on γ and on the plasma frequency ω_p which in turn depends on the density of free carriers, on their effective mass and on other parameters. In order to obtain a metallic behaviour below a given value of frequency ω_c, the number of free carriers (n_e) must be at least equal to

$$n_{min} = \frac{\varepsilon_\infty \varepsilon_0 m^*}{e^2}(\omega_c^2 + \gamma^2) \quad (6)$$

This value can be obtained by setting the real part of eqn (5) equal to zero and by replacing in it the expression for the plasma frequency of eqn (2). Only under these conditions there can be the possibility for a particle of such material to exhibit LSPRs. The higher the density of carriers, the broader will be the range of frequencies for which the material will behave optically as a metal, as the crossover frequency ω_c will proportionally increase. The classical Drude damping (γ), in the context of a LSPR, can be correlated to the various scattering mechanisms, among which intraband transitions (*i.e.* transition from electron states at energies close to the Fermi level to empty states within the same band) play an important role. Some of these scattering events require assistance from phonons, in order to fulfil the overall conservation of momentum, and therefore one of the main quantum mechanical damping

mechanisms that can be contemplated by the ''classical'' Drude model in a bulk metal is the one due to electron–phonon scattering.[25] As one can see from eqn (6), stronger Drude damping (γ) and a larger mass for the carriers would require a higher number of free carriers to stay in the region of metallic behaviour. Drude damping, by its classical definition ($\gamma = e/(\mu m^*)$), can be minimized in principle by a high mobility and by a large carrier mass m^* (see also our discussion on carrier mass later in this review). However, in doped semiconductors μ is negatively affected by a large concentration of dopants, due to impurity scattering, and therefore heavy doping would increase Drude damping (see also ref. 12). The same holds for self-doped materials, as in them the distribution of vacancies is generally disordered in the lattice. Additional complications might arise in the presence of particles with domains of multiple phases. Furthermore, in degenerate semiconductors the damping parameter, differently from metals, can be frequency dependent, due to scattering from ionized impurities.[26] These ions are always present in extrinsically doped semiconductors, and they are needed to balance the charge of the free carriers. An analysis of the scattering between free electrons and ionized impurities and its influence on the dynamic resistivity of tin doped indium oxide (ITO) has been reported by Hamberg and Granqvist.[27] Copper chalcogenides are however a notable exception, since the high value of the imaginary part of their high-frequency dielectric constant screens the free carriers from ionized impurities.[28] Consequently, there have been attempts to model the shape of the LSPR in these materials, using a frequency independent damping parameter.[28] More recent reports, however, would suggest otherwise,[29] and therefore this point has yet to be clarified.

At first approximation, the spectral position of the maximum in the LSPR does not depend on the NC size.[5] This is true as long as the NC size is such that optical retardation effects can be neglected. These effects are easily explained by considering that, in any material, the electric carriers feel the effect of each other after a time delay, which is set by the propagation speed of the electromagnetic field. If this time delay is comparable to or larger than the oscillation period of the external electric field, it is not possible to synchronize the motion of all of them. The LSPRs then shift to longer wavelengths, decrease in intensity and eventually disappear.[1] In metal NCs one can safely assume that for diameters below 20 nm retardation effects play a marginal role. In NCs of doped semiconductors the limit is proportionally higher due to their lower resonant frequency. Also, in larger nanoparticles multipolar modes start being active and radiation damping too must be taken into account.[1]

Losses in plasmonic NCs

In the Drude model, the imaginary part of the permittivity represents the losses of the material and it increases with decreasing frequency (*i.e.* with increasing wavelength). Therefore, at high frequencies, the metal should exhibit lower losses due to intraband transitions. This model however is oversimplified for real metals, as it does not take into account the actual band structure of the material. The imaginary term in the Drude model can describe well the losses due to intraband transitions in a wide range of frequencies, as discussed above. On the other hand, in some materials there might be a frequency threshold above which intraband transitions are not possible. This could happen if there is an energy gap between the partially filled band and a higher energy empty band. Also, if the plasmonic resonance is in a spectral region for which interband transitions are energetically possible, there will be additional optical losses that will contribute with an additional term to the imaginary part of the permittivity. These are obviously not included in the Drude model (in principle these transitions can be modelled as a set of Lorentz oscillators). This is, for example, the case of gold NCs, if they are embedded in a medium with low refractive index, as can be seen from Fig. 1, in particular the spectra calculated for $\varepsilon_m = 1$ and $\varepsilon_m = 2$. All these losses, which we have just described, contribute to increase the width of a LSPR, which is one of the most important parameters, since it sets the maximum near field enhancement that can be obtained from a plasmonic particle.[1] Stated alternatively, the plasmon dephasing time, which is inversely proportional to the width of the LSPR, should be as long as possible for all those applications which rely on local field enhancement, like for example surface enhanced Raman spectroscopy.[30] In this respect it is useful to introduce the concept of a ''quality factor'' (Q-factor) of the plasmonic resonance, which can be defined as the ratio of the LSPR resonance frequency over its linewidth.[31]

The minimization of losses in plasmonic NCs is a technologically relevant question, but how to achieve it? As we previously discussed, in a Drude metal the imaginary part of the permittivity is proportional to the square of the plasma frequency, hence to the number of free carriers, and it depends heavily on the damping constant γ. In the hunt for alternative plasmonic materials, one could seek to minimize losses (ε'') by reducing γ and/or the number of free carriers (to reduce the plasma frequency), clearly with the constraint that the number of carriers needs to stay over the threshold set by the crossover frequency, for the material to behave as a metal. This is a bit facilitated by a lower carrier mass, since the mass term appears in the denominator of the expression of the plasma frequency (eqn (2)). Overall, to minimize losses, one should engineer a material such that its plasmonic response occurs in a range of energies at which both intraband and interband transitions are not particularly significant[32] (see also ref. 12).

Theories for modelling the plasmonic response

For the case of spherical NCs of any size, the optical response can be still derived analytically by writing the incident radiation field in terms of spherical harmonics, and by imposing boundary conditions at the dielectric–metal interfaces. The resulting expressions are traditionally referred to as the ''Mie theory''.[1,24] Spheroids are also analytically treatable, and for this reason they are often used to describe the response of elongated NCs (rods and wires) and of disk and platelet shaped NCs, which can be considered as extreme cases of spheroids.[24] In rods

(disks) with circular cross sections the resonances are split into two modes: a transverse (out-of-plane) mode and a longitudinal (in-plane) one, the latter at lower energy.

The Mie theory is strictly valid only under certain assumptions, which are as follows: the particles are not mutually interacting (low volume fraction) and intrinsic size effects are negligible (*i.e.* the discretization of the electronic levels for very small NCs is not considered).[2] Another approximation implicit in the Mie theory is that the medium in which the particles are embedded is transparent near the LSPR region.[2] Alternatively, mean field approaches, like for instance the Maxwell-Garnett theory (MG), can be useful for describing moderately dense assemblies, in which the particles interact *via* their far fields.[33] Mendelsberg *et al.*[28] verified that, for two representative extrinsically doped and "self-doped" plasmonic NCs, namely ITO NCs and $Cu_{2-x}Se$ NCs, the Mie and MG theories give indeed similar results when used to simulate absorption spectra with NC volume fractions lower than 0.01. In the same work, it was shown that the MG theory can predict how the frequency and the width of the LSPRs of NCs are affected by sample inhomogeneity, like statistical distributions of geometrical size and number of free carriers.[28] In this context, a moderate (5–15%) size distribution affects only slightly the shape of the LSPR. The particle-to-particle variation of the free carrier density, on the other hand, can result in a significant broadening of the resonance.[28] Still in the same work, it was highlighted how the carrier density extracted by fitting the optical spectra with the Mie theory does not necessarily coincide with the concentration of dopant/vacancies, due to the presence of trap states and possibly of spurious crystal phases in the NCs.[28] When direct coupling of neighbouring particles becomes significant, more complex theories must be employed, such as the coupled multipoles method or the discrete dipole approximation.[2] These methods compute both the near and the far field interaction between NCs, and therefore they are more suited for investigating the coupling of plasmonic modes that appear in dense aggregates.[2] Since these theories provide explicit solutions to the Maxwell equations, they are computationally demanding.[2]

Electronic properties of degenerately doped semiconductor NCs

In order to better understand the plasmonic properties of degenerately doped semiconductors, it is useful to recall some basic aspects of their band structure. The optical bandgap, for degenerately doped p-type semiconductors, is defined as the difference between the bottom of the conduction band and the highest occupied state in the valence band. Conversely, for n-type semiconductors the optical bandgap is the difference between the highest occupied state in the conduction band and the top of the valence band. Fig. 2 exemplifies the case for typical n-type and p-type semiconductors. In both cases the optical bandgap depends on the free carrier concentration. This is the Burstein–Moss effect, and it can be explained by considering that, in semiconductors, the bandgap corresponds to the photon energy required to promote an electronic transition from the top of the valence band to the bottom of the conduction band. In degenerately doped n-type semiconductors (Fig. 2a), the lowest energy levels of the conduction band

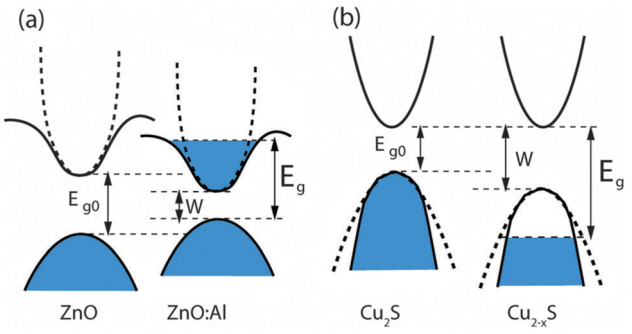

Fig. 2 Band structures of plasmonic semiconductor nanocrystals. (a) The intrinsic bandgap of aluminium-doped zinc oxide is smaller than the one of undoped zinc oxide, but the optical bandgap is increased, due to the state filling effect.[35] The curvature of the conduction band decreases, and consequently the effective mass increases, with increasing carrier density;[35] (b) in self-doped copper sulfide both the intrinsic and the optical bandgaps become larger when the doping level is increased.[36] The curvature of the valence band increases as the Fermi energy level decreases, and therefore the effective mass drops as the number of vacancies increases.[37]

are not available, because they are already occupied by electrons from the dopants. The optical bandgap is therefore increased by the difference between the energy of the highest occupied state and the bottom of the conduction band. A similar argument can also be outlined for p-doped semiconductors. In this case the highest energy levels of the valence band are populated by the extra holes (Fig. 2b). The energy of the highest occupied electron states in the valence band is therefore lower than it would be in the undoped material, which leads to an increase of the optical bandgap. For a parabolic conduction band the Burstein–Moss contribution depends on the carrier density *via* a term that is proportional to $(n_e)^{2/3}$.[27]

The Burstein–Moss effect is partly counterbalanced by many-body effects[27] which tend to shrink the bandgap, due to the contribution of scattering (electron–electron and electron–impurity) to the self-energy of the carriers.[27] Finally, since the plasmonic frequency of degenerately doped semiconductors is often used to back-calculate the carrier density, it is also important to note that the carrier density enters the formula for the plasmon frequency also implicitly, *via* the effective mass. Indeed, since electronic bands are never perfectly parabolic, when the doping level is increased, the new carriers feel a different curvature than the ones at the bottom of the band. Therefore, the effective mass of the free carriers depends on their concentration (see Fig. 2).[28] As a note of caution, the effective mass approximation loses validity far from the stationary points of the band.[34]

Copper chalcogenide NCs

Electronic and optical properties

Materials such as copper chalcogenides, tin and zinc oxides are characterized by a direct bandgap, which determines their optical properties in the visible range, and in some cases

($Cu_{2-x}Se$) also by an indirect bandgap.[17,18] We start the discussion here on self-doped binary copper chalcogenides ($Cu_{2-x}S$, $Cu_{2-x}Se$ and $Cu_{2-x}Te$), which are p-type semiconductors, and then move on with the other materials in the following sections. In copper chalcogenides, the top of the valence band has a strong contribution from the chalcogen p orbitals. The bottom of the conduction band has mainly contributions from Cu 4s and 4p orbitals (see for example the case of $Cu_{2-x}Se$).[38] We can assume that each Cu atom contributes to bonding with one 4s electron, while each chalcogen atom contributes with six p electrons. In a fully stoichiometric Cu_2E compound, the valence band is completely filled and the material would behave as an intrinsic semiconductor. When a Cu atom is removed from the lattice, a hole is created in the top of the valence band. As this has major contribution from the chalcogen, hole creation will mainly affect the valence of the chalcogen. X-ray photoelectron spectroscopy (XPS) studies on bulk films have indeed shown that in fully stoichiometric copper chalcogenides the valence of the chalcogen is −2 and that of copper is +1. In the corresponding sub-stoichiometric compounds, while the valence of copper remains +1, the chalcogen has a valence that is higher than −2.[39] This was also structurally related, at least for $Cu_{2-x}S$ and $Cu_{2-x}Se$, to the formation of S_2 (or Se_2) pairs. For $Cu_{2-x}S$, a limiting case is represented by CuS (*i.e.* $x = 0$), the mineral covellite, in which sulfur is present as both S^{-2} and S_2^{-2}.[40] For $Cu_{2-x}Se$, this is the mineral klockmannite (CuSe). At least in CuS, the valence of Cu is highly debated: some studies have assumed monovalent copper, others have indicated the presence of both Cu(I) and Cu(II), and recent experiments and calculations have set the valence of Cu to a value between 1 and 1.5 (see ref. 41 and citations therein). Covellite, which has strong p-type metallic character, should have therefore the highest concentration of free carries in the copper sulfide class of materials. Covellite NCs are indeed characterized by a strong free carrier absorption in the NIR region.[42,43] The peculiar structure of this material can be described as a stacking of trilayers, each of them composed of a layer of triangular CuS_3 units, sandwiched between two layers made of CuS_4 tetrahedra. Each trilayer is then bound to adjacent trilayers by disulphide bonds.[44] Electronic structure calculations and the evidence of anisotropic conductivity suggest that covellite does not behave as a 3D metal, but rather as a collection of 2D metal sheets staked perpendicular to the *c*-axis (of either the hexagonal or the orthorhombic modification of covellite, depending on the temperature).[45] This has interesting implications for the plasmonic properties of NCs of this material, as we shall discuss later in this review.

Synthesis, chemical transformations and applications in imaging, hyperthermia and sensing

The chemical synthesis of copper chalcogenide NCs has been described in several articles in the last few years.[15,22,46–54] For example, Zhao *et al.* reported the synthesis of $Cu_{2-x}S$ NCs using three methods: sonoelectrochemical, hydrothermal and solventless thermolysis. Similar optical properties of the particles were obtained from the three methods.[47] Representative absorption

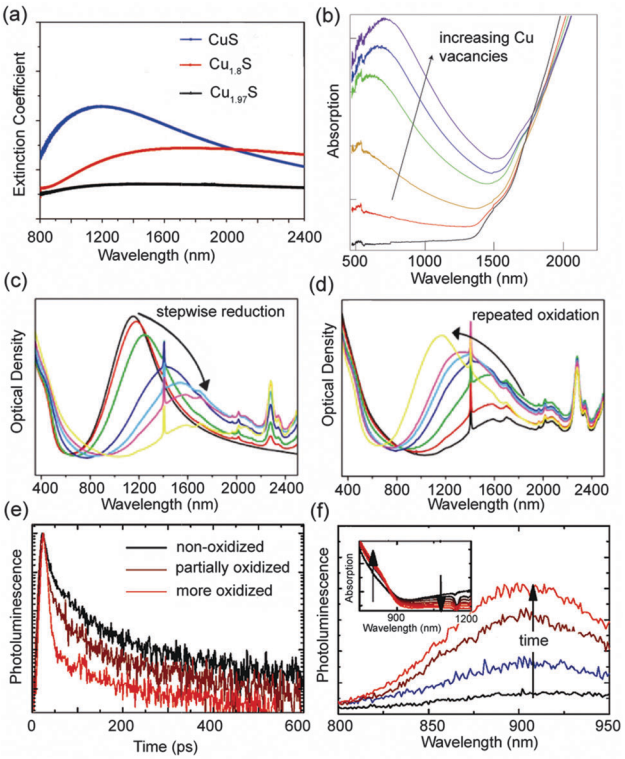

Fig. 3 Optical properties of self-doped copper chalcogenides. (a) Extinction spectra of $Cu_{2-x}S$ NCs, prepared sonoelectrochemically, in samples of different Cu stoichiometries, in the NIR region; (b) absorption spectra of $Cu_{2-x}S$ NCs, covering also the UV-vis region, from which both plasmonic and excitonic features can be seen. The plasmon resonance became more pronounced as the number of Cu vacancies was increased; (c) evolution of the LSPR of $Cu_{2-x}Se$ NCs as their composition was varied from $Cu_{1.81}Se$ to Cu_2Se by a step-wise reduction process; (d) the Cu stoichiometry could be decreased again, by means of an oxidation process: the oxidized particles exhibited again a LSPR; (e) the PL lifetime of $Cu_{2-x}S$ NCs (red curve) was shorter than that of the stoichiometric Cu_2S NCs; (f) also, the PL intensity from the same $Cu_{2-x}S$ NCs increased, while the intensity of their LSPR decreased, as their stoichiometry was restored to Cu_2S (inset). Panel (a) adapted with permission from ref. 47; copyright 2009 American Chemical Society. Panel (b) adapted with permission from ref. 48; copyright 2011 Macmillan Publishers Limited. Panels (c) and (d) adapted with permission from ref. 15; copyright 2009 American Chemical Society. Panels (e) and (f) adapted with permission from ref. 22; copyright 2012 American Chemical Society.

spectra of $Cu_{2-x}S$ samples synthesized sonoelectrochemically, with various Cu stoichiometries, are reported in Fig. 3a. This work of Zhao *et al.* started the field of plasmonic copper chalcogenide NCs. Djurelite $Cu_{2-x}S$ NCs of 2–6 nm size were prepared by Luther *et al.*, who additionally discussed their plasmonic properties.[48] These NCs have a free hole density of about 10^{21} cm^{-3}, which sets their LSPR energy in the NIR range, at roughly 0.7 eV. The quality factor of the plasmonic resonance was reported to be more than 3, a value that is comparable to what can be obtained with noble metal NCs.[48] Interestingly, Luther *et al.* were able to observe LSPR and excitonic transitions in the same NCs (see Fig. 3b).[48] Both features were shifted to higher energies when the number of vacancies was increased. According to the authors, the shift of the LSPR energy was due to the increased number of free carriers, and the shift of the

excitonic peak was caused by the Burstein–Moss effect. The synthesis and the properties of $Cu_{2-x}Se$ NCs were described in various papers.[15,22,49] Dorfs *et al.* for example synthesized fcc $Cu_{2-x}Se$ NCs and demonstrated reversible tuning of LSPR from 0.73 to 1.13 eV by means of redox processes:[15] Cu_2Se NCs were oxidized to $Cu_{1.6}Se$, by exposing them either to oxygen or to Ce(IV), and the reverse step was performed by adding excess Cu^+ ions, by which the plasmon resonance shifted to lower energies and finally it disappeared when the full Cu_2Se stoichiometry was re-established (Fig. 3c and d). In the study by Dorfs *et al.* the crystal structure of the samples did not change during the oxidation–reduction steps, despite the creation and annihilation of numerous copper vacancies.[15]

Kriegel *et al.* extended these studies to the whole family of copper chalcogenides ($Cu_{2-x}S$, $Cu_{2-x}Se$, $Cu_{2-x}Te$).[22] Differently from Dorfs *et al.*,[15] they used diisobutylaluminium hydride instead of Cu^+ ions as a reducing agent to quench the plasmon resonance and in their case the crystal structure did change during the reduction process. They attributed the stoichiometry change to a reduction of Cu^{2+} species inside the NCs to Cu^+, triggered by chemically injected electrons. By comparing the XRD and optical spectra recorded during the evolution of the NCs from the stoichiometric to the non-stoichiometric compound, they confirmed that the appearance of the LSPR was correlated with the introduction of copper vacancies in the NCs.[22] They also verified that the LSPR energy shifted to higher energies when the size of the NCs was reduced from 6 nm to 3 nm, a behaviour that is known in metal NCs and which is attributed to increased scattering of the free carriers with the NC surface as the size of the NCs decreases (see also the introductory section of this review on the Drude model).[1] They also monitored the fluorescence of $Cu_{2-x}S$ NCs as a function of the Cu stoichiometry (Fig. 3e and f). As expected, the fluorescence intensity dropped as the number of Cu vacancies increased, due to more efficient nonradiative recombination. The quenching of the fluorescence, which went hand in hand with the appearance of a LSPR, was attributed to several processes: Auger recombination, presence of trap states and exciton–plasmon energy transfer.[22]

Copper telluride NCs too have been investigated in detail. Yang *et al.*[50] and Li *et al.*[51] have reported protocols for preparing nearly monodisperse $Cu_{2-x}Te$ NCs with a variety of shapes,[50,51] and Li *et al.* were able to synthesize $Cu_{2-x}Te$ nanodisks.[55] NCs of alloys as well have been prepared:[52,53] in a recent work, for example, Dilena *et al.* developed a method for synthesizing $Cu_{2-x}S_ySe_{1-y}$ NCs with either cubic or hexagonal phase.[52a] According to them, the LSPR energy of these NCs depended mainly on the Cu stoichiometry and only slightly on the crystalline phase, or on the S/Se ratio.[52a] On the other hand, a more recent study by Liu *et al.* showed that by adjusting the synthesis conditions the LSPR of $Cu_{2-x}S_ySe_{1-y}$ NCs could be tuned between 1000 and 1600 nm (Fig. 4d).[53a,b] They found that the LSPR in copper sulfide and selenide NCs can be tuned by varying the capping ligand. For example, addition of oleylamine during synthesis red-shifts the LSPRS. This was attributed to trapping of surface holes by the deprotonated carboxylate group, which reduced the effective carrier concentration.

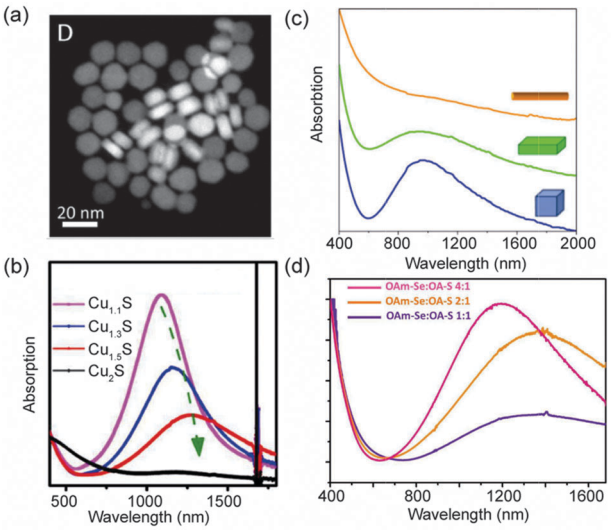

Fig. 4 (a) High angle annular dark field scanning TEM image of Cu_2S nanodisks; (b) evolution of the LSPR of $Cu_{2-x}S$ NCs, as the stoichiometry changed from $Cu_{1.1}S$ to Cu_2S; (c) absorption spectra of CuTe nanocubes, nanoplates and nanorods; (d) absorption spectra of $Cu_{2-x}S_{1-y}Sy$ alloy NCs synthesized using different oleylamine–Se/oleylamine–S molar ratios. Panels (a) and (b) reproduced with permission from ref. 56; copyright 2013 American Chemical Society. Panel (c) reproduced with permission from ref. 51; copyright 2013 American Chemical Society. Panel (d) reproduced with permission from ref. 53*a*; copyright 2013 American Chemical Society.

Applications of copper chalcogenide NCs have targeted mainly bio-imaging and photothermal therapy.[18,57] One of the first studies in this direction was the work of Hessel *et al.*, who have shown that $Cu_{2-x}Se$ NCs can convert 800 nm radiation into localized heating with the same efficiency as Au nanorods (Fig. 5a and b).[18] Clearly, the advantage of these NCs over Au nanorods is that in $Cu_{2-x}Se$ the LSPR *naturally* arises in the NIR and does not require any shape tuning. They made *in vitro* tests to check the biocompatibility of $Cu_{2-x}Se$ NCs and their efficacy against cancer cells. Song *et al.* coated $Cu_{2-x}Se$ NCs with a mesoporous silica ($mSiO_2$) shell to form Cu_9S_5@$mSiO_2$-PEG core–shell nanostructures.[58] These exhibited low toxicity and high blood compatibility and were used for a combined photothermal therapy and delivery of the anticancer drug doxorubicin. Liu *et al.* demonstrated the efficacy of $Cu_{2-x}Se$ NCs as contrast agents for photoacoustic tomography, which is a technique that combines optical excitation and ultrasound imaging of biological tissues (Fig. 5c).[59] Li *et al.* tested $Cu_{1.25}Te$ NCs for applications in imaging and phototherapy.[51] Particularly noteworthy is that the Nile red dye could be detected only with the $Cu_{1.25}Te$ NCs, and not even on the star-shaped Au NCs, which are one of the best materials for LSPR-enhanced bio-imaging.[51,60] This is because of the higher affinity of ketones (present in Nile red) for the surface of $Cu_{1.25}Te$ NCs than for that of Au NCs. Li *et al.* also got encouraging results on the potential application of $Cu_{1.25}Te$ NCs to phototherapy, although it was stated that further developments are needed to avoid the toxic release of Te atoms in the non-irradiated areas.[51] An interesting approach is to combine in one heterostructure a metallic and a doped semiconductor domain. Provided that both domains, when merged together, can retain their LSPRs, the heterostructure will exhibit high optical absorbance

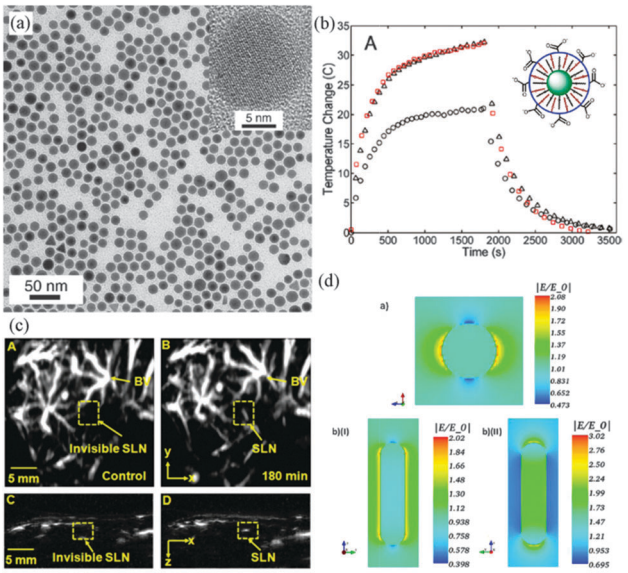

Fig. 5 (a) TEM image of $Cu_{2-x}Se$ NCs; (b) steady state heating data for Au nanoshells (black circles), Au nanorods (black triangles), and $Cu_{2-x}Se$ NCs (red squares), upon excitation with an 800 nm light source. The $Cu_{2-x}Se$ NCs of the experiments were encapsulated in an amphiphilic polymer shell, as sketched in the inset; (c) *in vivo* photoacoustic images of a sentinel lymph node (SLN) in a rat. (A) is a pre-injection image and (B) is collected 180 minutes after the injection of $Cu_{2-x}Se$ NCs. (C) and (D) are the corresponding depth-resolved scan images of (A) and (B); (d) calculated near-field enhancement maps for a $Cu_{2-x}Te$ sphere (top) and a nanorod (bottom). Panels (a) and (b) reproduced with permission from ref. 18; copyright 2011 American Chemical Society. Panel (c) reproduced with permission from ref. 59; copyright 2013 Wiley. Panel (d) reproduced with permission from ref. 29; copyright 2013 American Chemical Society.

and near-field enhancement in a wider frequency range. A step forward in this direction has been made by Liu *et al.*, who synthesized Au–$Cu_{2-x}Se$ heterostructures and demonstrated their use as contrast agents in dark field and photoacoustic imaging.[61]

One reason for using plasmonic NCs as markers for imaging is the possibility to leverage the enhancement of the non-linear optical processes near the surface of the NCs. Unfortunately, the near field enhancement (NFE) from copper chalcogenide NCs is expected to be much lower than that of noble metal NCs, due to the smaller number of free carriers, which in principle makes them less suitable than noble metal NCs for applications such as surface enhanced Raman scattering, metal enhanced fluorescence and plasmonic solar cells.[62] Kriegel *et al.* for example calculated the NFE for $Cu_{2-x}Te$ NCs of various shapes and, in the case of nanorods, they found it to be about 30 times lower than that of gold NCs (Fig. 5d).[29] On the other hand, the work of Li *et al.* discussed earlier on $Cu_{1.25}Te$ NCs[51] shows that hopes are not entirely lost in this direction, especially when molecule/ligand affinity is higher for the surface of copper chalcogenide NCs than for that of gold NCs.

In analogy with the findings of Liu *et al.*,[53] a recent recent work by Jain *et al.*[63] has shown how common ligands bound to the surface of $Cu_{2-x}S$ NCs can electronically dope the NCs, by charge transfer, which leads to a red shift and weakening of their LSPR.[63] More in general, they were able to show that oxidizing conditions, which would increase the number of free carriers, are indeed translated into an increased conductivity of a film of $Cu_{2-x}S$ NCs. The conductivity could be then reversibly decreased under reducing conditions. Jain *et al.* proposed that this property could be exploited for plasmonic detection of several chemical processes.[63]

Imaging, sensing and photothermal therapy do not conclude the range of potential application for copper chalcogenide NCs. NCs of these materials, because of their intrinsic ability to undergo cation exchange,[64] might be exploited for the sequestration of toxic metal ions in solution. This is however accompanied by the release of Cu ions. On the other hand covellite NCs have been shown by Yi *et al.* to incorporate Cu(I) ions in a reducing environment. If this incorporation can be extended to other metal ions, covellite NCs (and likewise Klockmannite CuSe and perhaps also CuTe NCs) could be in principle exploited as sequestrating agents for these species, without having to release Cu ions in return.

Shape dependent optical properties

In analogy with the case of metal nanoparticles, non-spherical NCs of copper chalcogenides, like nanodisks and nanorods, are expected to have multiple plasmonic resonances. In reality, conflicting claims have been made in this area. As already discussed above, Li *et al.* synthesized $Cu_{2-x}Te$ nanocubes and nanoplatelets with LSPR centred around 900 nm, while they did not find any LSPR for the $Cu_{2-x}Te$ nanorods (Fig. 4c).[51] In a recent work, rod and tetrapod shaped $Cu_{2-x}Te$ NCs were synthesized by Kriegel *et al.*[29] These NCs, as well as $Cu_{2-x}S$, $Cu_{2-x}Se$ and core–shell $Cu_{2-x}Se$–$Cu_{2-x}S$ NCs having rods or even more elaborate shapes, can be easily fabricated from the corresponding cadmium chalcogenide NCs by cation exchange.[64–68] All these anisotropic NCs exhibited weak longitudinal LSPRs (for the tetrapods clearly each arm should have a longitudinal LSPR), in contrast with predictions from the Drude model.[29] Accordance with experimental spectra was found by Kriegel *et al.* either by assuming significant damping (within the Drude model) for oscillations at wavelengths longer than 1000 nm (for $Cu_{2-x}Te$), or better by adopting a Lorentz model of localized oscillators.[29] This suggests that a large fraction of the holes in these copper-deficient chalcogenides is actually localized. It was therefore concluded that the shape of the NCs has little influence on their plasmonic response. It appears reasonable to expect that the possibility of treating the holes as free carriers reflects the degree by which the valence band could be approximated as parabolic. Indeed, the Drude-like approximation loses progressively validity as the concentration of free holes is increased and the Fermi energy level is shifted deeper inside the valence band. In this regard, it is interesting that Kriegel *et al.*[29] found that the longitudinal LSPR is damped for the whole family of copper chalcogenides, regardless of the density of free carriers. According to them, the partial localization of the carriers in copper chalcogenide nanorods could also be related to structural disorder,[29] in particular to the existence of a mobility edge, which would cause the localization of the holes with energy below a certain threshold.[29]

On a similar note, efforts have been undertaken to identify the possible presence of multiple LSPRs in nanodisks of copper

chalcogenides. $Cu_{2-x}Se$ nanodisks (diameter about 20 nm, thickness 3 nm) had been already synthesized by Choi *et al.*,[69] but their optical properties in the NIR were not discussed. More recently, Hsu *et al.* reported the synthesis of $Cu_{2-x}S$ nanodisks[70] and observed two optical absorption bands (one at 1800 and the other at 3100 nm), which they attributed to an out-of-plane longitudinal and in-plane plasmon mode, respectively. Differently from what could be expected based on the theory,[1] both LSPRs were blue shifted as the aspect ratio of the nanodisks was increased. This shift was attributed to the fact that the NCs with higher aspect ratios also had higher free carrier densities. Indeed, in order to increase the aspect ratio, the NCs were exposed for a longer time to high temperatures. According to the authors, this led to an increased concentration of copper vacancies and consequently to a higher carrier density. In another work, Xie *et al.* synthesized disk-shaped covellite (CuS) NCs *via* a hot-injection route and studied in detail their optical behaviour.[71] In these NCs, due to the peculiar 2D metallic character of covellite (as discussed earlier), the plasmonic behaviour can be considered as a set of in-plane collective hole oscillations, one for each metallic sheet that are stacked on top of each other in a disk. Xie *et al.* did not find compelling evidence of an additional optical absorption besides the broad band peaked at 1300 nm. They modelled the plasmonic response of the NCs, using the discrete dipole approximation, through which they were able to demonstrate that the in-plane longitudinal mode dominates the optical response, while the transverse out-of-plane mode is of much lower intensity and its signature is almost completely buried in the signal from the in-plane mode. This was additionally confirmed by the fact that the NIR peak red-shifted with increasing aspect ratio of the disks. In a following work, Xie *et al.* developed an approach to prepare $Cu_{2-x}S$ NCs with various stoichiometries, from covellite NCs up to Cu_2S NCs (Fig. 4a and b).[56] Their approach consisted of reacting the as-synthesized covellite NCs with a Cu(I) complex, by which a stepwise increase in the Cu stoichiometry could be achieved. In all these NCs, due to the gradual change in the LSPR intensity and spectral position from covellite on, such resonance was attributed to an in-plane mode (Fig. 4b). Along this line, Liu *et al.* synthesized digenite $Cu_{1.8}S$ NCs, which underwent a gradual transformation to covellite CuS upon aging (over a few days).[72] Consequently, their plasmonic properties too evolved to those of covellite NCs. A recent report on LSPR of CuS nanodisks by Wei *et al.* demonstrated reversible tunability of the LSPR *via* oxygen absorption and desorption.[73] The oxygen acted as an electron acceptor, and therefore it increased the hole concentration and blue-shifted the LSPR. The process could be reversed by ligand re-passivation, which caused oxygen desorption.[73] As klockmannite (CuSe) has a crystal structure that is closely related to that of covellite, it is likely that also in NCs of this material the plasmonic mode perpendicular to the planes of highest conductivity will be weak.

Plasmon dynamics

Studies on the plasmon dynamics of copper chalcogenide NCs have been reported by various groups already.[22,71,74–76]

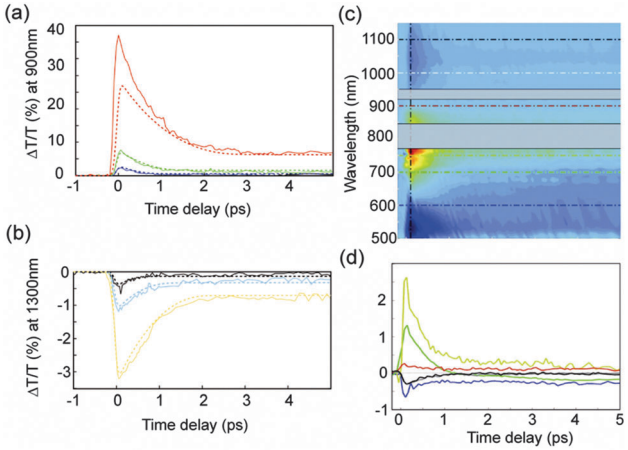

Fig. 6 (a) Transient absorption signal of $Cu_{2-x}Se$ NCs measured at the peak of the LSPR resonance and (b) at the red side of it. The solid lines of different colours refer to transient absorption signals recorded at different values of the pump power. The dashed lines are simulated traces obtained using the two temperature model; (c) time-wavelength map of the transient absorption signal ($\Delta T/T$) of $Cu_{1.75}Se$ NCs dispersed in toluene; (d) cross sections of the map reported in panel (c), for different probe wavelengths. Panels (a) and (b) reproduced with permission from ref. 74; copyright 2011 American Chemical Society. Panels (c) and (d) reproduced with permission from ref. 75; copyright 2011 American Chemical Society.

Scotognella *et al.* showed that the dynamical optical properties of $Cu_{2-x}Se$ NCs can be empirically modelled within the free electron approximation and the two-temperature model (TTM, see Fig. 6c and d).[74] This model was initially developed in order to rationalize the transient optical response of metals, after the absorption of sub-picosecond laser pulses,[74] and it considers electrons and phonons as two thermal reservoirs in thermodynamic equilibrium. Although this assumption is not strictly valid until the electrons have reached internal equilibrium (about 200 fs after laser excitation) the TTM could qualitatively reproduce the transient optical response of metal NCs.[21] It is known that in metals the TTM can be improved by considering the free carriers as divided into two groups: a thermal one, which follows the Fermi–Dirac distribution, and a non-thermal one for which the temperature is not defined.[77,78] Recently, Della Valle *et al.* demonstrated that this result holds also for copper chalcogenides, and that considering the contribution of the non-thermal carriers is essential for describing the evolution of the LSPR spectrum of $Cu_{2-x}Se$ NCs recorded with a pump–probe experiment (Fig. 6c and d).[75] Similar to metals, the optical spectrum of doped semiconductors near the LSPR frequency is dominated by the free carriers. Therefore, it is not surprising that they could also be modelled by the TTM.[74]

The results by Scotognella *et al.* on $Cu_{2-x}Se$ NCs[74] were confirmed and extended by Kriegel *et al.* to $Cu_{2-x}S$ and $Cu_{2-x}Te$ NCs.[22] By means of broadband pump–probe spectroscopy they found that the shape and the relaxation dynamics of the LSPR have strong analogies with those of noble metal NCs.[74] Broadly speaking, when the photon energy of the pump beam is below the onset of interband transitions, the optical properties are dominated by intra-band transitions and the interband ones only

contribute with an offset to the dielectric permittivity.[74] In this case the pump energy is entirely absorbed by the free carriers, leading to the formation of a non-thermal hot electron population, which thermalizes to a Fermi–Dirac distribution after a few hundreds of femtoseconds.[21] On the picosecond time scale, the electrons exchange energy with the lattice. On longer time scales (>10 ps), the heat is dissipated to the environment.[21] The LSPR depends both on the electron and on lattice temperature, and therefore it is strongly modulated in a pump–probe experiment. As shown by Scotognella *et al.*,[74] the modulations of the LSPR width observed in pump–probe experiments are significantly bigger than those observed in metals, under the same experimental conditions. This suggests that these chalcogenide NCs have extremely high optical nonlinearities, which could be exploited for applications in telecommunication devices. Interesting applications are also envisaged in fields such as all-optical ultra-fast switching and nonlinear nano-sensing.

On a different note, Xie *et al.* carried out transient absorption experiments at LSPR wavelengths on CuS nanodisks, and were able to identify coherent excitation of symmetric radial breathing modes.[71] These are well known to occur in NCs of noble metals,[79] but this is the first time that they had been identified in copper chalcogenide NCs.

Kriegel *et al.* synthesized CdTe–$Cu_{2-x}Te$ nano-heterostructures by partial cation exchange of Cd^{2+} with Cu^{+} ions in CdTe NCs.[76] The two sub-units were characterized by a type-II alignment and had poor electronic interactions, most likely due to the low spectral overlap between the CdTe exciton and the $Cu_{2-x}Te$ plasmon, but likely also because of substantial carrier localization in the $Cu_{2-x}Te$ domain, as discussed previously (*i.e.* the ''free'' carriers are not entirely delocalized in $Cu_{2-x}Te$). On the other hand, the CdTe exciton decay (probed by pump–probe spectroscopy) was faster in the heterostructure than in ''CdTe-only'' NCs. The decay was faster in heterostructures with longer $Cu_{2-x}Te$ domains, an effect that Kriegel *et al.* correlated with the increased probability of Auger recombination promoted by the presence of $Cu_{2-x}Te$, with its high density of carriers. Such effect is indicative of non-negligible spillage of the CdTe electron wavefunction in the $Cu_{2-x}Te$ domain.

Germanium telluride

Germanium telluride NCs are promising materials in the context of active plasmonics. They are known to exhibit a fast amorphous–crystalline phase transition which can be electrically triggered.[80,81] Recently, Polking *et al.* demonstrated that GeTe NCs are non-stoichiometric materials exhibiting LSPR, but only in the crystalline phase.[81] The authors were able to switch on and off the LSPR multiple times, by slowly heating and cooling down the NCs. One possible evolution of research in this direction would be to investigate the optical switching of the amorphous-crystalline transition. Driving the transition optically could eventually lead to the development of new types of ultrafast switchable plasmonic materials.[81]

Metal nitrides

In the hunt for the optimal material for plasmonics, it has been recently noted that some semiconductors could perform better than noble metals in certain applications. Transition metal nitrides (TiN) are among the most promising materials in this context:[19] they can sustain high free carrier concentrations (10^{22} cm^{-3}), which allows them to operate at visible and near-infrared frequencies (see for example ref. 82 and references therein). Moreover, their optical properties can be tuned by adjusting the processing conditions.[19] The absorption spectra of TiN NCs, calculated in the quasi-static approximation, have been reported by Naik *et al.*[12] With respect to other transition metal nitrides, TiN has smaller interband losses in the red side of the visible spectrum[82,83] and, for this reason, its performance as plasmonic material is comparable to that of noble metals, like gold and silver.[82] For example, the electric field enhancement at the surface of a TiN NC, due to LSPR, is only 10% smaller than that for gold.[82] Also, the real permittivity of TiN is smaller than that of noble metals due to its lower carrier concentration:[82] this characteristic makes it more suitable for applications in the emergent field of transformation optics.[82] For an overview on the plasmonic properties of TiN nanostructures and a discussion on their suitability for devices, see M. B. Cortie *et al.*[84] A few studies have reported the synthesis of TiN NCs to date.[85–90] TiN nanorods and nanosheets have also been fabricated: Joshi *et al.* synthesized TiN nanorods by low temperature solid-state metathesis of Ti(III),[91] while Huang *et al.* reported the synthesis of 3 nm thick TiN sheets.[92] It appears however that colloidal approaches to TiN nanoparticles, especially in the form of stable colloidal suspensions, need intensive development before their plasmonic properties can be studied in detail.

Another interesting material is InN. Palomaki *et al.* reported the synthesis of InN NCs with sizes between 4 and 10 nm.[93] These NCs have a direct bandgap at 0.7 eV and a LSPR at about 3000 nm. The free charges that contribute to the LSPR originate from the presence of positively charged surface states, which act as electron donors.[94] This makes it possible to readily tune the free carrier density of the NCs by surface chemistry.[93] Palomaki *et al.* succeeded indeed in reversibly tuning the LSPR frequency of InN NCs by about 200 nm by oxidizing them with $NOBF_4$ and subsequently reducing them with Bu_4NBH_4.[93]

Extrinsically doped n-type metal oxide NCs

Tin doped indium oxide (ITO)

The optical properties of tin-doped indium oxide (ITO) NCs have been investigated by various groups, as they belong to the intensively studied class of transparent conductive oxides.[26,95,96] The position of the plasmonic resonance of ITO can be varied from 1600 nm to 2200 nm by controlling the concentration of Sn dopants (see Fig. 7a–c)[95,97] or electrochemically by applying a bias voltage (Fig. 7d).[98] Like other wide band gap n-type semiconductors, the plasmonic band of ITO can be modelled *via* the Mie theory using a frequency dependent

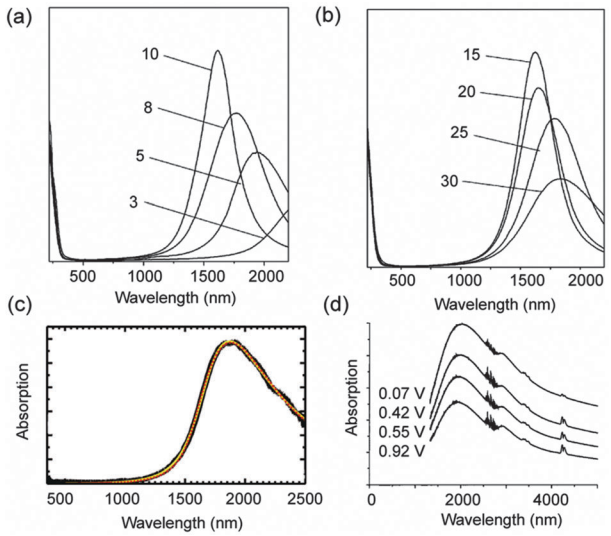

Fig. 7 Absorption spectra of ITO NCs doped with (a) 3–10% Sn and (b) 15–30% Sn (c); absorption spectrum of ITO NCs; (d) absorption spectra of a SnO_2:Sb electrode as a function of the applied potential. Panels (a) and (b) adapted with permission from ref. 95; copyright 2009 American Chemical Society. Panel (c) adapted with permission from ref. 28; copyright 2012 American Chemical Society. Panel (d) adapted with permission from ref. 98; copyright 2000 American Chemical Society.

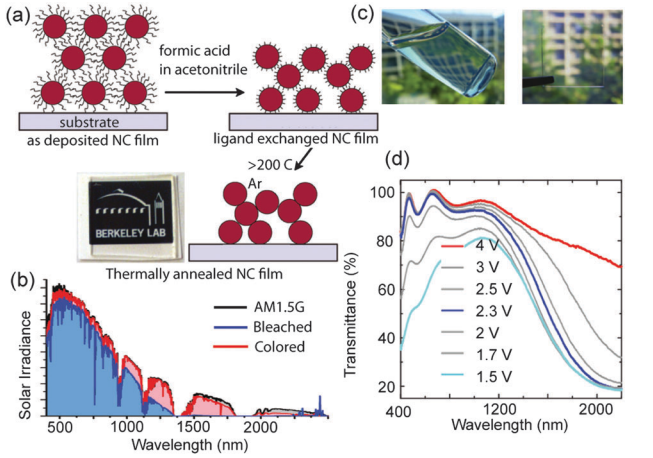

Fig. 8 (a) Process of depositing ITO NCs on quartz and the resulting film; (b) solar spectrum (AM 1.5G) modulated after transmission through a 310 nm thick ITO NC film in the bleached (lower infrared absorbance) and the coloured (higher infrared absorbance) states; (c) an aqueous solution of ITO NCs stabilized by polyniobate clusters (left) and ITO-in-NbO_x film on a glass substrate; (d) optical transmittance of a ITO-in-NbO_x film, as a function of the applied voltage. Panels (a) and (b) adapted with permission from ref. 14; copyright 2011 American Chemical Society. Panels (c) and (d) reproduced with permission from ref. 101; copyright 2013 Macmillan Publishers Limited.

damping parameter that describes scattering from ionized impurities.[26,27,99,100] Wang *et al.* noted however that the plasmon resonance appeared only for the body-centered cubic (bcc) NCs but not for the rhombohedral ones.[96] According to their interpretation, the crystal phase affects in a different way the two competing mechanisms that determine the optical bandgap: widening of the gap due to filling up of the conduction band states, and shrinking of the gap due to many-body effects. The plasmon appeared only when the first contribution was dominant, as in the case of cubic ITO NCs.[96]

A plasmon electrochromic effect on ITO NCs was also recently shown by Garcia *et al.*, who demonstrated dynamic and reversible doping of ITO NC films by electrochemically modulating the concentration of electrons in these NCs,[14] such that their plasmonic response could be readily tuned. As a result, the transmittance in the NIR of a film of these NCs could be dynamically modulated (Fig. 8). This concept was nicely extended to the fabrication of nanocomposite glasses made of ITO NCs dispersed in an amorphous NbO_x matrix, which exhibited a peculiar electrochromic switching ability: depending on the applied voltage, the glass went from fully transparent, to selective IR blocking, to blocking of both IR and visible light (Fig. 8c and d).[101] Remarkably, at an optimal 43% loading of ITO NCs in the film, the optical response of the composite in the visible, which in principle should be dictated only by the NbO_x matrix, was much higher than that of a pure NbO_x glass, indicating a structure of NbO_x, when combined with ITO NCs, that was substantially different from that of the pure NbO_x case.

Zinc oxides and tin oxides

Various groups have demonstrated the possibility of doping zinc oxide with several elements (mainly Al). Shim *et al.* for example observed enhanced IR absorption in n-type ZnO NCs, obtained by charge-transfer doping or by irradiating the crystals with above-bandgap UV light.[102] Faucheaux *et al.* were able to induce a LSPR by UV irradiation (Fig. 9d).[103] According to their report, the LSPR could be sustained by as few as four photoexcited charges, and could be switched off by exposing the NCs

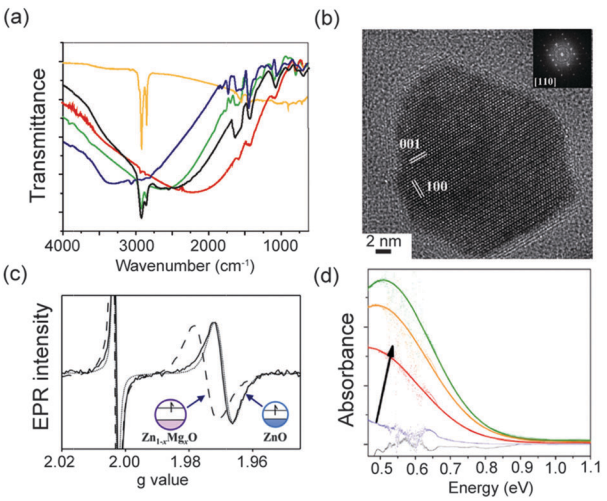

Fig. 9 AZO NCs. (a) FTIR spectra of AZO NCs characterized by different Al doping levels; (b) HRTEM image of a single AZO NC and, in the inset, the relative fast Fourier transform indicating the wurtzite crystal structure for this NC; (c) room temperature EPR signal of 2.9 nm ZNO NCs (dotted line), of 4.0 nm $Zn_{0.75}Mg_{0.25}O$ NCs (dashed line) and of an equimolar mixture of them (solid line); (d) photoinduced LSPR absorption in ZnO NCs. Panels (a) and (b) adapted with permission from ref. 13; copyright 2011 American Chemical Society. Panel (c) adapted with permission from ref. 113; copyright 2012 American Chemical Society. Panel (d) reproduced with permission from ref. 103; copyright 2013 American Chemical Society.

to oxygen. It is clearly established that Al-doped zinc oxide (AZO) NCs exhibit an infrared plasmon peak (see Fig. 9a). These materials may become a cheaper and less toxic alternative to ITO NCs for applications in flexible and wearable electronic devices. Synthesis routes to AZO NCs and related studies on the optical properties have been published by various groups.[100,104–107] Buonsanti *et al.* reported the synthesis of high quality AZO NCs with sizes tunable between 5 and 20 nm (see Fig. 9a and b). Their method allows for independently tuning the crystal size and the doping level.[13] In general, these two parameters are correlated, since the concentration of impurities is higher near the surface of the crystals.[13] By varying the concentration of Al dopants between 0 and 8%, the plasmon resonance could be tuned between 3 and 10 microns (1000 to 3200 cm^{-1}), while keeping the NCs transparent in the visible range.[13] AZO nanorods and wires too should be promising as plasmonic materials.[108] One of the first studies was reported by Kusinski *et al.*, who synthesised AZO nanowires by dissolving Zn acetate and Al acetate in tri-octylamine.[108] The authors investigated how the doping level affects the morphology and the electrical properties of the NCs. While undoped zinc oxide is an insulator, it becomes conductive with the addition of Al atoms. In Kusinski's experiments, the highest conductivity was obtained with a concentration of Al atoms of about 1% and, for higher doping levels, the conductivity decreased due to the formation of defect states.[108]

Besides doping, an additional approach to make ZnO NCs conductive is to negatively charge them upon illumination with UV light. This photo-chemical method has been described and investigated by Schimpf *et al.* using EPR.[110] Photochemically charged ZnO NCs have the same optical properties as the Al doped ones. The main difference is that, in photochemically charged NCs, the extra charges are compensated by protons instead of Al ions. Since protons provide lower binding energy than Al ions, the photochemically charged NCs are more reactive and, in particular, more susceptible to oxidation.[110] Whitaker *et al.* measured the EPR signal from NCs of different sizes, and compared the various gyromagnetic ratios. In this way they could prove that extra electrons were indeed added to the conduction band of the NCs.[111] They corroborated this conclusion by showing that, when charged and uncharged NCs were mixed together, the charge only flew from smaller NCs to bigger NCs.[112] Indeed, because of quantum confinement, the conduction band of small NCs is higher in energy than that of larger NCs.[112] Therefore, when two NCs are brought in contact, extra charges (electrons) can flow from smaller to larger NCs, but not *vice versa*.[112]

The synthesis of In-doped ZnO NCs was described by Hammarberg *et al.*[105] and isovalently doped colloidal $Zn_{1-x}Mg_xO$ were synthesized by Gamelin *et al.*,[113] who highlighted the possibility of tuning the reduction potential of ZnO by varying the concentration of Mg dopants, which could have important implications for redox chemistry.[113] They also found that the addition of Mg^{2+} ions increased the bandgap and shifted the visible-defect luminescence to higher energies. Electron paramagnetic resonance (EPR) spectra indicated that the extra carriers belonged to the conduction band and therefore they were delocalized throughout the NC (Fig. 9c).

Zum Felde *et al.* investigated the infrared optical properties of Antimony-doped tin oxide (ATO) NCs synthesized by a co-precipitation method.[98] ATO is a transparent conductive material which is characterized by good chemical stability and good electron conductivity and, for these reasons, it has been the subject of intense investigation.[114] Zum Felde *et al.* were able to modulate the conductivity and the infrared absorption of ATO NCs by applying a bias voltage and obtained a controllable and reversible electro-chromic effect.[98] Interestingly, in their experiments the plasmon peak did not shift but its amplitude changed as a function of the external voltage. The apparent reason was that the bias voltage did not affect the density of carriers but rather their mobility.[98]

Cadmium oxide

Rocksalt cadmium oxide is a n-type degenerate semiconductor, with an indirect bandgap of about 0.84 eV and a direct one that can be tuned from 2.2 eV to 3.1 eV by adding dopants (see ref. 109 and references therein). Its intrinsic conductivity is relatively high for an oxide and, although its origin is still debated, it appears that the major contribution comes from intrinsic defects: mainly Cd interstitial and oxygen vacancies (V_O).[109] The free carrier density in CdO can be increased, by doping with In, up to 10^{21} cm^{-3}.[115] Gordon *et al.* synthesized monodispersed spherical (8.0 ± 1.0 nm in size) and octahedral shaped (51.0 ± 3.6 nm in size) In:CdO NCs by thermal decomposition of cadmium acetylacetonate.[115] They showed that these materials, in addition to being characterized by a relatively high carrier concentration, have a quality factor higher than that of other typical ''non-noble metal'' plasmonic NCs, such as $Cu_{2-x}S$ and $WO_{2.83}$ (see the following section on tungsten oxide).[115] The LSPR was between 1.8 μm and 3.5 μm, depending on the doping concentration and the dielectric environment. The high environmental sensitivity of these NCs (150 nm per unit of refractive index change) should be a key asset for their use as plasmonic sensors. Also, their LSPR appears to depend non-linearly on the carrier concentration, and to approach a saturation value at high doping levels.[115] According to Gordon *et al.*, the reason for the nonlinearity is that, at higher doping levels, the scattering rate between free carriers and In atoms is increased.[115] The authors found a doping limit of 6% for octahedral and 20% for spherical In:CdO NCs. When attempting to dope the NCs above this limit they observed a decrease in the shape uniformity of the resulting NCs.[115]

Oxygen-deficient metal oxide NCs

Tungsten oxide

Differently from the copper chalcogenide cases discussed earlier in this review, in which copper vacancies create holes in the valence band, often in oxygen-deficient metal oxide NCs self-doping translates into the presence of electrons in the conduction band (therefore n-doping) which has mainly contribution from the metal orbitals. We discuss first tungsten oxide (WO_3) NCs. These are ideal candidates for photochemical applications,

because they are stable and have a bandgap (2.6 eV) suitable to collect solar light and which can be tuned by varying the oxygen stoichiometry.[116] In particular, oxygen deficient WO_{3-x} NCs have intense absorption in the visible and near-IR region of the spectrum, due to a tunable LSPR. Despite there are many known stable bulk phases for this oxide with different stoichiometries, only a few of them have been investigated at the nanoscale. For instance, Manthiram *et al.* showed that the optical absorption spectrum of $WO_{2.83}$ NCs can be tuned from 1.38 eV (900 nm) to 1.13 eV (1100 nm), by heating the NCs in the presence of oxygen, a process which leads to the incorporation of new oxygen atoms in the crystal lattice and therefore modifies the carrier density.[116] The same authors pointed out that the LSPR sensitivity of $WO_{2.83}$ NCs, expressed as wavelength shift per unitary change of the environment refractive index, appeared to be comparable to that of noble metals, but the quality factor was not as high.[116] Therefore, their local field enhancement is expected to be weaker than that of noble metal nanoparticles.

Molybdenum oxides

Molybdenum trioxide (MoO_3) is a n-type semiconductor with a bandgap of about 3 eV; it has orthorhombic crystal structure and has already found technological application in various fields, most notably in heterogeneous catalysis.[117] MoO_3 is a layered material, formed by a sequence of bilayers oriented perpendicular to the [010] direction.[117] There are several known phases of oxygen deficient molybdenum oxide (MoO_{3-x}): Mo_4O_{11}, Mo_8O_{23}, and Mo_9O_{26}. They are all characterized by a strong blue colour arising from a NIR absorption band.[118,119] Huang *et al.* published a colloidal synthesis of MoO_{3-x} nanosheets (3 nm thick, 100–1000 nm wide) exhibiting NIR LSPR (at 900 nm). To compensate for oxygen deficient stoichiometry, part of Mo atoms in the lattice have valence equal to 5, and in each of these cases one free electron is added to the d band, as demonstrated by Huang *et al.* using EPR and XPS.[118] Also, in analogy with copper chalcogenide NCs, in which the LSPR can be tuned by means of redox processes, Huang *et al.* were able to progressively quench the plasmon resonance in these MoO_{3-x} sheets *via* oxidation in air.[118] Most likely this process re-established a MoO_3 composition in the sheets. These materials too were proposed for use in photothermal therapy, as the irradiation of solutions of nanosheets in cyclohexane with a NIR (980 nm) laser induced a rise in temperature that could not be attributed to the sole contribution of direct heating of the solvent.

NCs of other transition metal oxides

Rhenium oxide

We now move to the description of other renowned oxide NCs exhibiting LSPR. One notable example is rhenium oxide (ReO_3), which might find applications in plasmonics, due to its remarkably high conductivity, close to the one of metallic copper.[120] ReO_3, in analogy with WO_3, is an octahedrally coordinated transition metal oxide (MO_6) and belongs to the wider class of perovskites, which we will briefly discuss in the conclusions and outlook section. A simple understanding of the metallic properties of ReO_3 can be made by comparing its electronic structure with that of the "hypothetical" WO_3 compound with a cubic structure as that of ReO_3 (WO_3 exhibits several temperature induced phase transitions, up to a tetragonal phase, but never a cubic one).[121] The calculated band structures for the two materials are topologically very similar.[121] However, in stoichiometric WO_3 (non-oxygen deficient) the valence band is completely filled and the conduction band is empty, and indeed WO_3 behaves as a semiconductor (as discussed above). In ReO_3, on the other hand, as Re has one more d electron than W, this extra electron per Re atom is placed in the conduction band, which becomes half-filled. Isoelectronic with ReO_3 is indeed the $NaWO_3$ bronze (see also the section on conclusions and outlook).[121] The LSPR of ReO_3 NCs lies in the visible range and it can be tuned by varying the NC size, from 490 nm (NC size of 8.5 nm) to 540 nm (NC size of 32 nm).[120] Various types of core–shell NCs with ReO_3 core and shell made of Au, Ag, SiO_2 or TiO_2 were also reported.[122]

An interesting aspect of ReO_3 is that it combines optical and magnetic properties. The magnetic properties of ReO_3 NCs appear to be size dependent: while bigger (30 nm) NCs are diamagnetic, smaller ones (8.5 nm) are paramagnetic, due to uncompensated surface spin.[120] Therefore this material may find application in magneto-plasmonics, especially due to the significant size-dependence of the magnetic and plasmonic properties.

Transition metal dioxides

The so-called "strongly correlated materials" are a class of compounds the physical properties of which cannot be accurately described by considering electrons as independent.[123–125] They can feature a variety of phenomena, superconductivity and giant magneto-resistance being among the most known examples.[123] Among them, transition metal oxide NCs have been investigated in detail. In the context of plasmonics, it is worth remembering that many metal oxides are characterized by intrinsic conductive behaviour and can potentially be plasmonic. However, understanding the plasmonic properties of transition metal oxides requires more sophisticated methods than the ones developed for noble metal NCs. This could be one of the reasons why plasmonic NCs of transition metal oxides have not received as much attention as NCs of noble metals. Nevertheless, NCs of a wide variety of transition metal dioxides (such as CuO_2, RuO_2, IrO_2, OsO_2, VO_2) have been synthesized[126] and a few of them have been found to possess LSPRs. One example is vanadium oxide (VO_2), which is an interesting material because it has a temperature dependent plasmonic resonance.[123] At room temperature, VO_2 is an insulator and therefore it cannot have plasmonic properties. Around 340 K, it has a conductor–insulator phase transition, above which LSPRs are clearly recognizable.[127] In perspective, it would be useful to be able to reduce the transition temperature of VO_2 (for example by doping) in order to match specific applications, like for instance optical switching, optical recording and smart windows.[128,129] Optical switching applications of VO_2 NCs are

possible as the insulator–conductor transition can be triggered by irradiation with laser pulses. The use of short laser pulses for controlling the phase transition of VO_2 has been the subject of intensive studies, especially for what concerns the bulk,[130] but much less on the side of NCs. It is nowadays quite established that the conductive phase of VO_2 can be switched on optically in less than 100 fs.[131] The photo-generation of holes in the valence band, induced by a near-infrared laser pulse, triggers a phase transition into a conductive state and the appearance of a LSPR.[127,132] Since this process is non-thermally activated, it is very fast and the switching speed is generally limited by the temporal width of the laser pulse. However, the reverse transition to the insulator state is a thermal process and it is much slower (in the range of nanoseconds) because it is limited by how fast heat can diffuse out of the NC sample.[127]

In one of the few studies published so far on VO_2 NCs, Rini *et al.* reported a pump–probe investigation on VO_2 NCs and nanorods grown by ion implantation and self-assembly in silica.[127] More recently there has been interest in the synthesis of VO_2 nanowires and in VO_2 nanowires doped with tungsten or hydrogen (see ref. 123 and references therein). Nanostructuring a strongly correlated material, like VO_2, and embedding it in a device could in principle open up new avenues to exploit its properties. For instance the LSPR could be tuned by applying high electric fields through the use of nanoelectrodes.[123] In a field-effect transistor type of configuration, for example, it should be possible to use the gate voltage to control the carrier density inside the NCs, therefore driving a phase transition, although in the specific case of VO_2 there has been so far little success in this direction.[123] VO_2, being a phase changing material, could be incorporated into transparent matrixes to realize smart windows that block infrared solar radiation. In this regard, Zhou *et al.* proposed a way to exploit the temperature dependent LSPR of VO_2–SiO_2 core–shell nanostructures to realize thermochromic windows.[128] The authors could in this way modulate the transmitted solar energy in the near-IR range by about 20%.[128]

Extrinsically doped "traditional" semiconductor NCs and NCs of other materials

Doped silicon

Much work has gone into doping "traditional" semiconductor materials (group IV and III–V semiconductors) in order to obtain the high density of free carriers necessary to make them plasmonic.[12] Particular appealing materials are those with high carrier mobility, for example GaAs, as this allows a reduction of the density of free carriers required to achieve metallic behaviour in a given frequency range. On the other hand, silicon is one of the most popular materials in the electronic industry and, despite that it has an indirect bandgap, it also finds applications in photonics. The possibility of doping silicon to endow it with plasmonic resonances is therefore desirable. On the other hand, one has to keep in mind that the reliable synthesis of NCs of doped semiconductors still poses challenges. For example, it has been traditionally difficult to synthesize plasmonic Si NCs, due to issues in achieving substitutional doping.[133] Recently, however, Rowe *et al.* were able, *via* a nonthermal plasma technique, to synthesize phosphorus doped Si NCs, with a LSPR between 0.007 and 0.3 eV.[133] The size of the NCs was between 4 and 10 nm. They consisted of a crystalline core coated with a 1 nm thick amorphous phase. About one-third of the phosphorus atoms were located in the crystalline core, each of them contributing with a free carrier. Smaller NCs had a higher density of free carriers and a more blue-shifted LSPR. Smaller NCs on the other hand had also a more irregular and faceted shape, which led to increased surface scattering and broadened the LSPR.[133]

Conclusions and outlook

We have summarized in this review the main types of emerging plasmonic NCs, alternative to the more traditional cases of Au, Ag, and Cu, and highlighted their synthesis, properties and potential applications. The list of materials, properties and applications is far from being complete, as highlighted by the increasing number of papers appearing in this fast growing field. There is obviously a plethora of additional materials that could exhibit LSPRs. In principle, all materials having conductive behaviour are potential candidates. Many oxides, in addition to those covered in the previous sections, fall into this category, although it is likely that in most of them strong damping due to losses will prevent the observation of a clear plasmonic behaviour. Most of these oxides have n-type conductivity, but some, for example those belonging to the delafossite class of compounds, are p-type conductors.[134] NCs of these materials would have interesting applications in transparent electrodes. In this context, there has been interest in materials which can act as hole-injectors. Among them, nickel oxide, a p-type transparent semiconductor, has been one of the most investigated members.[135–137]

In the class of metal oxides, A_2BO_4 spinels are certainly important members. It has been recently demonstrated by Paudel *et al.* that neither oxygen vacancies nor cation vacancies can be the leading source of conductive behaviour in spinels.[138] What really counts is the presence of metal-on-metal anti-site substitutions (metal anti-sites), that is, defects in which a site that would be occupied by an A cation is actually occupied by a B cation (B-on-A, or B_A), and the other way around (A-on-B, or A_B). This type of defect is common in spinels, as both cations tend to have similar orbital radii. The possibility of releasing carriers (electrons or holes) is related to the ability of a cation to maintain its valence when moved from its home site. When for example, in a normal III_2–II–VI_4 spinel, a B-on-A defect is formed, the low-valent B cation is moved from a tetrahedral site (T_d) to an octahedral site (O_h). If its valence remains +2, this will lead to an acceptor level, capable of releasing holes. If its valence is instead changed to +3, its energy level will move up, deep into the conduction band and it will become an electrically

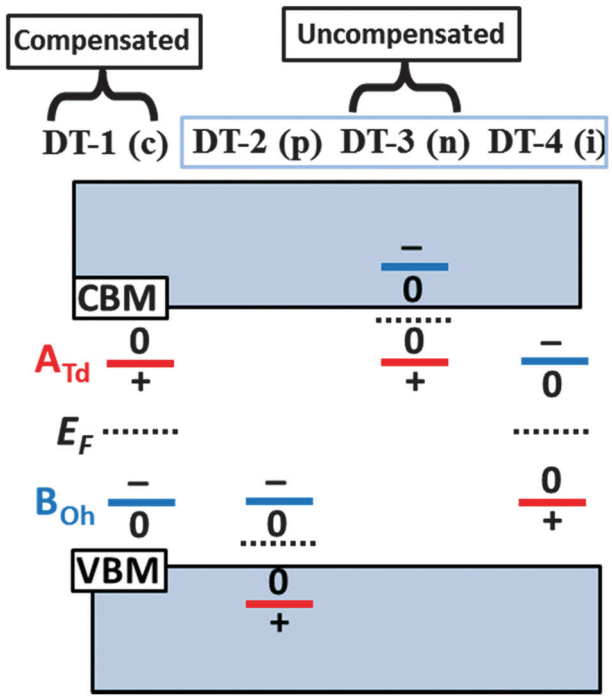

Fig. 10 Different doping types, for a A_2BO_4 spinel, arising from the relative energetic positions of the donor A-on-T_d (in red) and acceptor B-on-O_h (blue) defects: compensated (DT1); p-type (DT2), n-type (DT3); intrinsic (DT4). Adapted with permission from ref. 138; copyright 2011 Wiley.

neutral defect. Oppositely, when an A-on-B defect is formed, the high-valent A cation is moved from an O_h site to a T_d site. If its valence remains +3, it will lead to a donor level, capable of releasing electrons. If its valence is changed to +2, its energy level will move down, deep into the valence band and the defect will become electrically neutral. Depending on whether the energy of the donor is above that of the acceptor, or only acceptors are present, or only donors, or finally whether the energy of the acceptor is above that of the donor, we can have four distinct types of doping types (DTs), as shown in Fig. 10. In DT1, both defects are electrically active and compensate each other, whereas in DT2 and DT3 only one defect is active, leading to either p (DT2) or n type (DT3) doping. In DT4, both defects are electrically active and uncompensated. The interesting point here is that, except for DT1, additional doping with external dopants can lead to a further increase in the number of free carriers. The extensive work of Paudel *et al.* shows that we are still at the beginning of understanding the electrical properties of this important class of materials.[138] Here, possible future scenarios in plasmonics too could be uncovered, especially if carrier densities can be pushed up significantly.

Another large class of materials is represented by perovskites, which have the general formula AMX_3.[139] They take the name from the mineral perovskite ($CaTiO_3$): its structure is formed by corner-sharing TiO_6 octahedra, with the large Ca^{2+} cation occupying the centre of the cell. While the ideal perovskite structure is cubic, there are many possible deviations from such symmetry, depending on the elements involved but also on the presence of vacancies. ReO_3, WO_3 and MoO_3 too belong to perovskites, actually to a subclass of them, in which the "A" cation sublattice has been entirely removed (*i.e.* they can be considered as $\square MX_3$ compounds). ReO_3, as we have discussed earlier, has plasmonic properties. On the other hand, a wide variety of metals can be intercalated in MoO_3 and WO_3, giving rise to the so-called molybdenum and tungsten bronzes, with their characteristic intense colours (depending on the stoichiometry of the intercalated metal) and metallic lustre.[119] These intercalation compounds have a strong metallic behaviour, especially at a high molar fraction of the intercalated metal, due to the transfer of electrons from the metal to the conduction band of MO_3 or WO_3. These intercalation materials are also of interest because of their quasi-2D metallic behaviour, arising from the highly anisotropic layered structures in this case, and also for their charge density wave-driven metal-to-insulator transitions at low temperatures. Other interesting bronzes have been reported in the past, in which the intercalated entities can also be molecules.[140] In general, perovskites can have many interesting properties, ranging from oxygen ion conduction often accompanied by electron conduction, to high temperature superconductivity and ferromagnetism, depending on their structure and composition. Important members are the $La_{1-x}SrMnO_3$ and $La_{1-x}SrCO_3$ perovskites, which exhibit temperature and magnetic field dependent conductivity (the latter arising from the mixed +3/+4 valence of the Mn or Co cations).[141,142] There are also members of the class that are known to be excellent electron conductors, and doped $ASnO_3$ (A = Ca, Sr, Ba) have been also proposed as candidate transparent conductors[139] (for example La-doped $BaSnO_3$).[143] Future studies in this direction might uncover plasmonic properties too.

There are many compounds that, depending on their stoichiometry/structure, can have either semiconducting or metallic behaviour, and we can cite only a few here. Some metal phosphides for example can be in this list. A recent study by G. Manna *et al.* on Cu_3P NCs has shown that also this class of phosphides can exhibit LSPRs, again most likely due to Cu vacancies.[144] The synthesis of this type of NCs has been intensively developed in the last few years by De Trizio *et al.*[145,146] Several copper chalcogenides, in addition to those already discussed in this review, are characterized by metallic conductivity. Another example, among the many, is represented by ternary compounds having the formula $MCu_{2n}X_{n+1}$ (M is alkali metal, X = S, Se, Te, $n = 1 \pm 3$). These have a "layered" structure, with Cu–S layers separated by a layer of alkali metals.[147] If all Cu species had +1 valence and the X species had −2 valence, there will be a net −2 charge per $[Cu_{2n}X_{n+1}]$ unit. Since the charge is actually −1 (compensated by a +1 charge of the alkali metal), then in analogy with the cases discussed earlier, the components, Cu and X, will have mixed valences. These compounds have a high density of holes (probably about one hole in the valence band for each $MCu_{2n}X_{n+1}$ unit) and they display a metallic behaviour. Therefore it might be useful to look into NCs of these materials for potential LSPRs. It is noteworthy to mention here also the class

of ternary $Cu_xFe_yS_z$ compounds. While most of them are intrinsic semiconductors, for example, $CuFeS_2$, $CuFeS_3$, $CuFe_2S_3$ and Cu_5FeS_4 (bornite),[148–152] their oxidation (often due to air exposure and most likely unintentional) leads to the formation of an absorption band in the NIR. This is probably plasmonic in origin, and should be due to the partial loss of Cu as a consequence of oxidation, although it has almost never been interpreted as such. It is not entirely excluded, however, that the NIR band arises mainly from the possible side formation of copper sulfide phases as a consequence of oxidation, as for example is found in the leaching of bornite.[153] Other potentially interesting ternary chalcogenides are the Cu–Sn–X (X = S, Se, Te) ones. For example, compounds like Cu_2SnS_3, $Cu_5Sn_2S_7$ and Cu_3SnS_4 are all traditionally known as intrinsic semiconductors. However, recent work has shown NIR absorption from them that may be indicative of a LSPR,[154] and also metallic conductivity in some cases.[155] Whether this absorption/conductivity truly originates from them (for example due to mixed valence of the anion sublattice) and is not due to spurious $Cu_{2-x}S$ phases or even to d–d transitions related to Cu(II) species is something that needs to be carefully validated in the future. In general, all these ternary compounds will require more scrutiny in the near future.

Chevrel phases are another class of compounds, with the formula $M_xMo_6X_8$ (with M being one among several possible elements, $1 < x < 4$, and X = S, Se, Te),[156] that have been investigated intensively because of the thermoelectric and low temperature superconducting behaviour of some of their members, as well as for energy storage applications. They can be considered as cage-like structures with a Mo_6X_8 cage that can be intercalated with various atoms. Depending on the number and valence of the atoms that can be intercalated in each site of the cage, these materials can possess either metallic or semiconducting behaviour. Reflectivity and complex magneto-optical Kerr-effect measurements on a series of Chevrel phases exhibiting metallic behaviour evidenced a carrier density of the order of 10^{21} cm^{-3}, comparable to that of many materials discussed above, for which NIR LPRS were observed in NCs.[157] The measurements however evidenced a heavy carrier mass (around 10 m_e) and strong damping.

In analogy to the case of layered metal oxides, transition metal dichalcogenides (TMDCs) are nowadays popular because of the many interesting evolutionary advances in physical properties when going from bulk materials to single layered nanosheets.[158–160] It is actually known since decades that intercalation of various organic and inorganic (for example alkali metals) species in between the layers can lead to a significant variation in their electronic properties.[161,162] Intercalation of hydrazine in TiS_2, $TiSe_2$ and ZrS_2, for instance, yields composite metallic materials with carrier concentrations up to 10^{22} cm^{-3}, due to charge transfer from hydrazine to the conduction band of the host TMDC.[162] Similar carrier densities have been found for example in $LiTiS_2$.[161] Recently, hydrogen-incorporated TiS_2 nanosheets with ultrahigh conductivity were reported.[163] NCs of such materials might exhibit plasmonic properties. Since colloidally stable few-layer nanodisks of some TMDCs can now be synthesized by chemical approaches,[164] it will be certainly interesting to attempt further manipulation of these NCs to eventually assess the presence of LSPRs.

As one can see, the whole field is under intense development. As new synthesis routes to NCs are being developed day by day in several laboratories, interesting developments can be expected in this direction for what concerns potential plasmonic properties in novel classes of NCs. One however should not forget that, even if plasmonic behaviour is found in a new material, besides fundamental science investigations, we should always strive towards some useful applications of it. If the material quickly degrades, or if the local field enhancement is weak because for example the density of free carriers is low and/or the carriers are localized, then in comparison with the traditional plasmonic materials the spectrum of possible applications for this new member may be restricted.

Acknowledgements

This work was supported in part by the EU FP7 ERC starting grant NANO-ARCH (contract no. 240111) and by the Italian FIRB grant (contract no. RBAP115AYN).

Notes and references

1 S. A. Maier, *Plasmonics: Fundamentals and Applications*, Springer, New York, NY, USA, 2007.
2 S. K. Ghosh and T. Pal, *Chem. Rev.*, 2007, **107**, 4797.
3 P. Zijlstra and M. Orrit, *Rep. Prog. Phys.*, 2011, **74**, 106401.
4 V. Giannini, A. I. Fernández-Domínguez, S. C. Heck and S. A. Maier, *Chem. Rev.*, 2011, **111**, 3888.
5 N. C. Lindquist, P. Nagpal, K. M. McPeak, D. J. Norris and S.-H. Oh, *Rep. Prog. Phys.*, 2012, **75**, 036501.
6 K. M. Mayer and J. H. Hafner, *Chem. Rev.*, 2011, **111**, 3828.
7 J. N. Anker, W. P. Hall, O. Lyandres, N. C. Shah, J. Zhao and R. P. Van Duyne, *Nat. Mater.*, 2008, **7**, 442.
8 M. Hu, J. Chen, Z.-Y. Li, L. Au, G. V. Hartland, X. Li, M. Marquez and Y. Xia, *Chem. Soc. Rev.*, 2006, **35**, 1084.
9 P. K. Jain, X. Huang, I. H. El-Sayed and M. A. El-Sayed, *Plasmonics*, 2007, **2**, 107.
10 The name ''antenna effect'' refers to the fact that, in conductive materials, the surface charge density and, therefore, the normal component of the electric field are highest near the points where the radius of curvature is minimal.
11 M. G. Blaber, M. D. Arnold and M. J. Ford, *J. Phys.: Condens. Matter*, 2010, **22**, 143201.
12 G. V. Naik, V. M. Shalaev and A. Boltasseva, *Adv. Mater.*, 2013, **25**, 3264.
13 R. Buonsanti, A. Llordes, S. Aloni, B. A. Helms and D. J. Milliron, *Nano Lett.*, 2011, **11**, 4706.
14 G. Garcia, R. Buonsanti, E. L. Runnerstrom, R. J. Mendelsberg, A. Llordes, A. Anders, T. J. Richardson and D. J. Milliron, *Nano Lett.*, 2011, **11**, 4415.
15 D. Dorfs, T. Härtling, K. Miszta, N. C. Bigall, M. R. Kim, A. Genovese, A. Falqui, M. Povia, L. Manna and H. Thomas, *J. Am. Chem. Soc.*, 2011, **133**, 11175.

16 A. L. Routzahn, S. L. White, L.-K. Fong and P. K. Jain, *Isr. J. Chem.*, 2012, **52**, 983.
17 Y. Zhao and C. Burda, *Energy Environ. Sci.*, 2012, **5**, 5564.
18 C. M. Hessel, V. P. Pattani, M. Rasch, M. G. Panthani, B. Koo, J. W. Tunnell and B. A. Korgel, *Nano Lett.*, 2011, **11**, 2560.
19 G. V. Naik, J. Kim and A. Boltasseva, *Opt. Mater. Express*, 2011, **1**, 1090.
20 N. W. Ashcroft and I. Mermin, *Solid State Physics*, Harcourt School, Orlando, FL, USA, 1987.
21 G. V. Hartland, *Chem. Rev.*, 2011, **111**, 3858.
22 I. Kriegel, C. Jiang, J. Rodríguez-Fernández, R. D. Schaller, D. V. Talapin, E. Da Como and J. Feldmann, *J. Am. Chem. Soc.*, 2012, **134**, 1583.
23 A. D. Rakic, A. B. Djurišic, J. M. Elazar and M. L. Majewski, *Appl. Opt.*, 1998, **37**, 5271.
24 C. F. Bohren and D. R. Huffman, *Absorption and Scattering of Light by Small Particles*, John Wiley & Sons, New York, NY, USA, 1983.
25 C. Voisin, N. Del Fatti, D. Christofilos and F. Vallée, *J. Phys. Chem. B*, 2001, **105**, 2264.
26 R. J. Mendelsberg, G. Garcia and D. J. Milliron, *J. Appl. Phys.*, 2012, **111**, 063515.
27 I. Hamberg and C. G. Granqvist, *J. Appl. Phys.*, 1986, **60**, R123.
28 R. J. Mendelsberg, G. Garcia, H. Li, L. Manna and D. J. Milliron, *J. Phys. Chem. C*, 2012, **116**, 12226.
29 I. Kriegel, J. Rodríguez-Fernández, A. Wisnet, H. Zhang, C. Waurisch, A. Eychmüller, A. Dubavik, A. O. Govorov and J. Feldmann, *ACS Nano*, 2013, **7**, 4367.
30 S. Schlücker, *Surface Enhanced Raman Spectroscopy: Analytical, Biophysical and Life Science Applications*, Wiley-VCH Verlag, Weinheim, 2011.
31 C. Sönnichsen, T. Franzl, T. Wilk, G. von Plessen, J. Feldmann, O. Wilson and P. Mulvaney, *Phys. Rev. Lett.*, 2002, **88**, 077402.
32 J. B. Khurgin and G. Sun, *Appl. Phys. Lett.*, 2010, **96**, 181102.
33 J. C. M. Garnett, *Philos. Trans. R. Soc. London, Ser. A*, 1906, **205**, 237.
34 P. Y. Yu and M. Cardona, *Fundamentals of Semiconductors*, Springer, Berlin, Heidelberg, New York, 2010.
35 J. S. Kim, J.-h. Jeong, J. K. Park, Y. J. Baik, I. H. Kim, T.-Y. Seong and W. M. Kim, *J. Appl. Phys.*, 2012, **111**, 123507.
36 P. Lukashev, W. Lambrecht, T. Kotani and M. van Schilfgaarde, *Phys. Rev. B: Condens. Matter Mater. Phys.*, 2007, **76**, 195202.
37 V. V. Gorbachev and I. M. Putilin, *Phys. Status Solidi A*, 1973, **16**, 553.
38 E. J. D. Garba and R. L. Jacobs, *Physica B+C*, 1986, **138**, 253.
39 J. C. W. Folmer and F. Jellinek, *J. Less-Common Met.*, 1980, **76**, 153.
40 B. Douglas, *J. Chem. Educ.*, 2009, **86**, 980.
41 I. I. Mazin, *Phys. Rev. B: Condens. Matter Mater. Phys.*, 2012, **85**, 115133.
42 S. K. Haram, A. R. Mahadeshwar and S. G. Dixit, *J. Phys. Chem.*, 1996, **100**, 5868.
43 Y. Du, Z. Yin, J. Zhu, X. Huang, X.-J. Wu, Z. Zeng, Q. Yan and H. Zhang, *Nat. Commun.*, 2012, **3**, 1177.
44 A. Casaca, E. B. Lopes, A. P. Gonçalves and M. Almeida, *J. Phys.: Condens. Matter*, 2012, **24**, 015701.
45 W. Liang and M. H. Whangbo, *Solid State Commun.*, 1993, **85**, 405.
46 N. J. Freymeyer, P. D. Cunningham, E. C. Jones, B. J. Golden, A. M. Wiltrout and K. E. Plass, *Cryst. Growth Des.*, 2013, **13**, 4059.
47 Y. Zhao, H. Pan, Y. Lou, X. Qiu, J. Zhu and C. Burda, *J. Am. Chem. Soc.*, 2009, **131**, 4253.
48 J. M. Luther, P. K. Jain, T. Ewers and A. P. Alivisatos, *Nat. Mater.*, 2011, **10**, 361.
49 S. Deka, A. Genovese, Y. Zhang, K. Miszta, G. Bertoni, R. Krahne, C. Giannini and L. Manna, *J. Am. Chem. Soc.*, 2010, **132**, 8912.
50 H.-J. Yang, C.-Y. Chen, F.-W. Yuan and H.-Y. Tuan, *J. Phys. Chem. C*, 2013, **117**, 21955.
51 W. Li, R. Zamani, P. Rivera Gil, B. Pelaz, M. Ibáñez, D. Cadavid, A. Shavel, R. A. Alvarez-Puebla, W. J. Parak, J. Arbiol and A. Cabot, *J. Am. Chem. Soc.*, 2013, **135**, 7098.
52 (*a*) E. Dilena, D. Dorfs, C. George, K. Miszta, M. Povia, A. Genovese, A. Casu, M. Prato and L. Manna, *J. Mater. Chem.*, 2012, **22**, 13023; (*b*) P. L. Saldanha, R. Brescia, M. Prato, H. Li, M. Povia, L. Manna and V. Lesnyak, *Chem. Mater.*, 2014, DOI: 10.1021/cm4035598.
53 (*a*) X. Liu, X. Wang and M. T. Swihart, *Chem. Mater.*, 2013, **25**, 4402; (*b*) X. Liu, X. Wang, B. Zhou, W.-C. Law, A. N. Cartwright and M. T. Swihart, *Adv. Funct. Mater.*, 2013, **23**, 1256.
54 W. Li, R. Zamani, M. Ibáñez, D. Cadavid, A. Shavel, J. R. Morante, J. Arbiol and A. Cabot, *J. Am. Chem. Soc.*, 2013, **135**, 4664.
55 H. Li, R. Brescia, M. Povia, M. Prato, G. Bertoni, L. Manna and I. Moreels, *J. Am. Chem. Soc.*, 2013, **135**, 12270.
56 Y. Xie, A. Riedinger, M. Prato, A. Casu, A. Genovese, P. Guardia, S. Sottini, C. Sangregorio, K. Miszta, S. Ghosh, T. Pellegrino and L. Manna, *J. Am. Chem. Soc.*, 2013, **135**, 17630.
57 Y. Li, W. Lu, Q. Huang, M. Huang, C. Li and W. Chen, *Nanomedicine*, 2010, **5**, 1161.
58 G. Song, Q. Wang, Y. Wang, G. Lv, C. Li, R. Zou, Z. Chen, Z. Qin, K. Huo, R. Hu and J. Hu, *Adv. Funct. Mater.*, 2013, **23**, 4281.
59 X. Liu, W. C. Law, M. Jeon, X. Wang, M. Liu, C. Kim, P. N. Prasad and M. T. Swihart, *Adv. Healthcare Mater.*, 2013, **2**, 952.
60 L. Rodríguez-Lorenzo, R. n. A. Álvarez-Puebla, I. Pastoriza-Santos, S. Mazzucco, O. Stéphan, M. Kociak, L. M. Liz-Marzán and F. J. García de Abajo, *J. Am. Chem. Soc.*, 2009, **131**, 4616.
61 X. Liu, C. Lee, W.-C. Law, D. Zhu, M. Liu, M. Jeon, J. Kim, P. N. Prasad, C. Kim and M. T. Swihart, *Nano Lett.*, 2013, **13**, 4333.
62 H. A. Atwater and A. Polman, *Nat. Mater.*, 2010, **9**, 205.
63 P. K. Jain, K. Manthiram, J. H. Engel, S. L. White, J. A. Faucheaux and A. P. Alivisatos, *Angew. Chem., Int. Ed.*, 2013, **52**, 13671.

64 H. Li, M. Zanella, A. Genovese, M. Povia, A. Falqui, C. Giannini and L. Manna, *Nano Lett.*, 2011, **11**, 4964.
65 D. H. Son, S. M. Hughes, Y. Yin and A. Paul Alivisatos, *Science*, 2004, **306**, 1009.
66 P. K. Jain, L. Amirav, S. Aloni and A. P. Alivisatos, *J. Am. Chem. Soc.*, 2010, **132**, 9997.
67 K. Miszta, D. Dorfs, A. Genovese, M. R. Kim and L. Manna, *ACS Nano*, 2011, **5**, 7176.
68 H. Li, R. Brescia, R. Krahne, G. Bertoni, M. J. P. Alcocer, C. D'Andrea, F. Scotognella, F. Tassone, M. Zanella, M. De Giorgi and L. Manna, *ACS Nano*, 2012, **6**, 1637.
69 J. Choi, N. Kang, H. Y. Yang, H. J. Kim and S. U. Son, *Chem. Mater.*, 2010, **22**, 3586.
70 S.-W. Hsu, K. On and A. R. Tao, *J. Am. Chem. Soc.*, 2011, **133**, 19072.
71 Y. Xie, L. Carbone, C. Nobile, V. Grillo, S. D'Agostino, F. Della Sala, C. Giannini, D. Altamura, C. Oelsner, C. Kryschi and P. D. Cozzoli, *ACS Nano*, 2013, **7**, 7352.
72 L. Liu, H. Zhong, Z. Bai, T. Zhang, W. Fu, L. Shi, H. Xie, L. Deng and B. Zou, *Chem. Mater.*, 2013, **25**, 4828.
73 T. Wei, Y. Liu, W. Dong, Y. Zhang, C. Huang, Y. Sun, X. Chen and N. Dai, *ACS Appl. Mater. Interfaces*, 2013, **5**, 10473.
74 F. Scotognella, G. Della Valle, A. R. Srimath Kandada, D. Dorfs, M. Zavelani-Rossi, M. Conforti, K. Miszta, A. Comin, K. Korobchevskaya, G. Lanzani, L. Manna and F. Tassone, *Nano Lett.*, 2011, **11**, 4711.
75 G. Della Valle, F. Scotognella, A. R. S. Kandada, M. Zavelani-Rossi, H. Li, M. Conforti, S. Longhi, L. Manna, G. Lanzani and F. Tassone, *J. Phys. Chem. Lett.*, 2013, **4**, 3337.
76 I. Kriegel, A. Wisnet, A. R. Srimath Kandada, F. Scotognella, F. Tassone, C. Scheu, H. Zhang, A. Govorov, J. Feldmann and J. Rodriguez-Fernandez, *J. Mater. Chem. C*, 2013, DOI: 10.1039/c3tc32049a.
77 W. S. Fann, R. Storz, H. W. K. Tom and J. Bokor, *Phys. Rev. B: Condens. Matter Mater. Phys.*, 1992, **46**, 13592.
78 C. K. Sun, F. Vallée, L. Acioli, E. P. Ippen and J. G. Fujimoto, *Phys. Rev. B: Condens. Matter Mater. Phys.*, 1993, **48**, 12365.
79 R. Krahne, G. Morello, A. Figuerola, C. George, S. Deka and L. Manna, *Phys. Rep.*, 2011, **501**, 75.
80 G. Bruns, P. Merkelbach, C. Schlockermann, M. Salinga, M. Wuttig, T. D. Happ, J. B. Philipp and M. Kund, *Appl. Phys. Lett.*, 2009, **95**, 043108.
81 M. J. Polking, P. K. Jain, Y. Bekenstein, U. Banin, O. Millo, R. Ramesh and A. P. Alivisatos, *Phys. Rev. Lett.*, 2013, **111**, 037401.
82 G. V. Naik, J. L. Schroeder, X. Ni, A. V. Kildishev, T. D. Sands and A. Boltasseva, *Opt. Mater. Express*, 2012, **2**, 478.
83 P. Patsalas and S. Logothetidis, *J. Appl. Phys.*, 2001, **90**, 4725.
84 M. B. Cortie, J. Giddings and A. Dowd, *Nanotechnology*, 2010, **21**, 115201.
85 J. Hu, Q. Lu, K. Tang, S. Yu, Y. Qian, G. Zhou and X. Liu, *J. Am. Ceram. Soc.*, 2004, **83**, 430.
86 X. Yang, C. Li, L. Yang, Y. Yan and Y. Qian, *J. Am. Ceram. Soc.*, 2003, **86**, 206.
87 H.-S. Hsueh, C.-T. Yang, J. I. Zink and M. H. Huang, *J. Phys. Chem. B*, 2005, **109**, 4404.
88 R. Aghababazadeh, A. R. Mirhabibi, B. Rand, S. Banijamali, J. Pourasad and M. Ghahari, *Surf. Sci.*, 2007, **601**, 2881.
89 P. P. George, A. Gedanken, S. B.-D. Makhlouf, I. Genish, A. Marciano and R. Abu-Mukh, *J. Nanopart. Res.*, 2008, **11**, 995.
90 B. Mazumder and A. L. Hector, *J. Mater. Chem.*, 2009, **19**, 4673.
91 U. A. Joshi, S. H. Chung and J. S. Lee, *J. Solid State Chem.*, 2005, **178**, 755.
92 T.-Y. Huang and C.-C. Chen, *J. Cryst. Growth*, 2008, **310**, 853.
93 P. K. B. Palomaki, E. M. Miller and N. R. Neale, *J. Am. Chem. Soc.*, 2013, **135**, 14142.
94 I. Mahboob, T. Veal, C. McConville, H. Lu and W. Schaff, *Phys. Rev. Lett.*, 2004, **92**, 036804.
95 M. Kanehara, H. Koike, T. Yoshinaga and T. Teranishi, *J. Am. Chem. Soc.*, 2009, **131**, 17736.
96 T. Wang and P. V. Radovanovic, *J. Phys. Chem. C*, 2011, **115**, 406.
97 J. G. Lu, S. Fujita, T. Kawaharamura, H. Nishinaka, Y. Kamada, T. Ohshima, Z. Z. Ye, Y. J. Zeng, Y. Z. Zhang, L. P. Zhu, H. P. He and B. H. Zhao, *J. Appl. Phys.*, 2007, **101**, 083705.
98 U. zum Felde, M. Haase and H. Weller, *J. Phys. Chem. B*, 2000, **104**, 9388.
99 A. Pflug, V. Sittinger, F. Ruske, B. Szyszka and G. Dittmar, *Thin Solid Films*, 2004, **455–456**, 201.
100 Z. Lu, J. Zhou, A. Wang, N. Wang and X. Yang, *J. Mater. Chem.*, 2011, **21**, 4161.
101 A. Llordes, G. Garcia, J. Gazquez and D. J. Milliron, *Nature*, 2013, **500**, 323.
102 M. Shim and P. Guyot-Sionnest, *J. Am. Chem. Soc.*, 2001, **123**, 11651.
103 J. A. Faucheaux and P. K. Jain, *J. Phys. Chem. Lett.*, 2013, **4**, 3024.
104 K. J. Chen, T. H. Fang, F. Y. Hung, L. W. Ji, S. J. Chang, S. J. Young and Y. J. Hsiao, *Appl. Surf. Sci.*, 2008, **254**, 5791.
105 E. Hammarberg, A. Prodi-Schwab and C. Feldmann, *J. Colloid Interface Sci.*, 2009, **334**, 29.
106 T. V. Thu and S. Maenosono, *J. Appl. Phys.*, 2010, **107**, 014308.
107 S. Suwanboon, P. Amornpitoksuk, A. Haidoux and J. C. Tedenac, *J. Alloys Compd.*, 2008, **462**, 335.
108 G. J. Kusinski, J. R. Jokisaari, R. Noriega, L. Goris, M. Donovan and A. Salleo, *J. Microsc.*, 2010, **237**, 443.
109 M. Burbano, D. O. Scanlon and G. W. Watson, *J. Am. Chem. Soc.*, 2011, **133**, 15065.
110 A. M. Schimpf, S. T. Ochsenbein, R. Buonsanti, D. J. Milliron and D. R. Gamelin, *Chem. Commun.*, 2012, **48**, 9352.
111 K. M. Whitaker, S. T. Ochsenbein, V. Z. Polinger and D. R. Gamelin, *J. Phys. Chem. C*, 2008, **112**, 14331.
112 R. Hayoun, K. M. Whitaker, D. R. Gamelin and J. M. Mayer, *J. Am. Chem. Soc.*, 2011, **133**, 4228.
113 A. W. Cohn, K. R. Kittilstved and D. R. Gamelin, *J. Am. Chem. Soc.*, 2012, **134**, 7937.

114 J. Zhang and L. Gao, *Inorg. Chem. Commun.*, 2004, **7**, 91.
115 T. R. Gordon, T. Paik, D. R. Klein, G. V. Naik, H. Caglayan, A. Boltasseva and C. B. Murray, *Nano Lett.*, 2013, **13**, 2857.
116 K. Manthiram and A. P. Alivisatos, *J. Am. Chem. Soc.*, 2012, **134**, 3995.
117 D. O. Scanlon, G. W. Watson, D. J. Payne, G. R. Atkinson, R. G. Egdell and D. S. L. Law, *J. Phys. Chem. C*, 2010, **114**, 4636.
118 Q. Huang, S. Hu, J. Zhuang and X. Wang, *Chem.–Eur. J.*, 2012, **18**, 15283.
119 M. Greenblatt, *Chem. Rev.*, 1988, **88**, 31.
120 K. Biswas and C. N. R. Rao, *J. Phys. Chem. B*, 2006, **110**, 842.
121 F. Corà, M. G. Stachiotti, C. R. A. Catlow and C. O. Rodriguez, *J. Phys. Chem. B*, 1997, **101**, 3945.
122 S. Ghosh, K. Biswas and C. N. R. Rao, *J. Mater. Chem.*, 2007, **17**, 2412.
123 E. Morosan, D. Natelson, A. H. Nevidomskyy and Q. Si, *Adv. Mater.*, 2012, **24**, 4896.
124 V. Anisimov and Y. Izyumov, *Electronic structure of strongly correlated materials*, Springer-Verlag, Berlin, Heidelberg, 2010.
125 D. N. Basov, R. D. Averitt, D. van der Marel, M. Dressel and K. Haule, *Rev. Mod. Phys.*, 2011, **83**, 471.
126 K. Biswas and C. N. R. Rao, *J. Nanosci. Nanotechnol.*, 2007, **7**, 1969.
127 M. Rini, A. Cavalleri, R. W. Schoenlein, R. López, L. C. Feldman, R. F. Haglund, L. A. Boatner, T. E. Haynes and J. R. F. Haglund, *Opt. Lett.*, 2005, **30**, 558.
128 Y. Zhou, A. Huang, Y. Li, S. Ji, Y. Gao and P. Jin, *Nanoscale*, 2013, **5**, 9208.
129 P. Jin, S. Nakao and S. Tanemura, *Thin Solid Films*, 1998, **324**, 151.
130 M. F. Becker, A. B. Buckman, R. M. Walser, T. Lépine, P. Georges and A. Brun, *J. Appl. Phys.*, 1996, **79**, 2404.
131 A. Cavalleri, T. Dekorsy, H. Chong, J. Kieffer and R. Schoenlein, *Phys. Rev. B: Condens. Matter Mater. Phys.*, 2004, **70**, 161102.
132 Z. Tao, T.-R. T. Han, S. D. Mahanti, P. M. Duxbury, F. Yuan, C.-Y. Ruan, K. Wang and J. Wu, *Phys. Rev. Lett.*, 2012, **109**, 166406.
133 D. J. Rowe, J. S. Jeong, K. A. Mkhoyan and U. R. Kortshagen, *Nano Lett.*, 2013, **13**, 1317.
134 F. Trani, J. Vidal, S. Botti and M. a. L. Marques, *Phys. Rev. B: Condens. Matter Mater. Phys.*, 2010, **82**, 085115.
135 B. Sasi, K. G. Gopchandran, P. K. Manoj, P. Koshy, P. Prabhakara Rao and V. K. Vaidyan, *Vacuum*, 2002, **68**, 149.
136 G. Boschloo and A. Hagfeldt, *J. Phys. Chem. B*, 2001, **105**, 3039.
137 F. Odobel, L. c. Le Pleux, Y. Pellegrin and E. Blart, *Acc. Chem. Res.*, 2010, **43**, 1063.
138 T. R. Paudel, A. Zakutayev, S. Lany, M. d'Avezac and A. Zunger, *Adv. Funct. Mater.*, 2011, **21**, 4493.
139 J. B. Goodenough, *Rep. Prog. Phys.*, 2004, **67**, 1915.
140 M. Greenblatt, *Acc. Chem. Res.*, 1996, **29**, 219.
141 G. Tang, Y. Yu, W. Chen and Y. Cao, *J. Alloys Compd.*, 2008, **461**, 486.
142 S. Yamaguchi, Y. Okimoto, K. Ishibashi and Y. Tokura, *Phys. Rev. B: Condens. Matter Mater. Phys.*, 1998, **58**, 6862.
143 S. Sallis, D. O. Scanlon, S. C. Chae, N. F. Quackenbush, D. A. Fischer, J. C. Woicik, J.-H. Guo, S. W. Cheong and L. F. J. Piper, *Appl. Phys. Lett.*, 2013, **103**, 042105.
144 G. Manna, R. Bose and N. Pradhan, *Angew. Chem., Int. Ed.*, 2013, **52**, 6762.
145 L. De Trizio, F. De Donato, A. Casu, A. Genovese, A. Falqui, M. Povia and L. Manna, *ACS Nano*, 2013, **7**, 3997.
146 L. De Trizio, A. Figuerola, L. Manna, A. Genovese, C. George, R. Brescia, Z. Saghi, R. Simonutti, M. Van Huis and A. Falqui, *ACS Nano*, 2012, **6**, 32.
147 V. A. Starodub, *Russ. Chem. Rev.*, 1999, **68**, 801.
148 P. Kumar, S. Uma and R. Nagarajan, *Chem. Commun.*, 2013, **49**, 7316.
149 A. M. Malyarevich, K. V. Yumashev, N. N. Posnov, V. P. Mikhailov and V. S. Gurin, *Appl. Phys. B: Lasers Opt.*, 2000, **70**, 111.
150 A. M. Malyarevich, N. N. Posnov, I. A. Denissov, K. V. Yumashev, V. P. Mikhailov and V. S. Gurin, *Proc. SPIE, ICONO '98*, 1999, vol. 3735, p. 121.
151 V. S. Gurin, *Colloids Surf., A: Physicochemical and Engineering Aspects*, 1998, **142**, 35.
152 A. M. Wiltrout, N. J. Freymeyer, T. Machani, D. P. Rossi and K. E. Plass, *J. Mater. Chem.*, 2011, **21**, 19286.
153 J. E. Dutrizac, T. T. Chen and J. L. Jambor, *Metall. Trans. B*, 1985, **16**, 679.
154 Z. Su, K. Sun, Z. Han, F. Liu, Y. Lai, J. Li and Y. Liu, *J. Mater. Chem.*, 2012, **22**, 16346.
155 C. Wu, Z. Hu, C. Wang, H. Sheng, J. Yang and Y. Xie, *Appl. Phys. Lett.*, 2007, **91**, 143104.
156 J. K. Burdett and J. H. Lin, *Inorg. Chem.*, 1982, **21**, 5.
157 P. Fumagalli and J. Schoenes, *Phys. Rev. B: Condens. Matter Mater. Phys.*, 1991, **44**, 2246.
158 M. Xu, T. Liang, M. Shi and H. Chen, *Chem. Rev.*, 2013, **113**, 3766.
159 Q. H. Wang, K. Kalantar-Zadeh, A. Kis, J. N. Coleman and M. S. Strano, *Nat. Nanotechnol.*, 2012, **7**, 699.
160 M. Chhowalla, H. S. Shin, G. Eda, L.-J. Li, K. P. Loh and H. Zhang, *Nat. Chem.*, 2013, **5**, 263.
161 C. M. Julien, *Mater. Sci. Eng., R*, 2003, **40**, 47.
162 A. M. Ghorayeb and R. H. Friend, *J. Phys.: Condens. Matter*, 1987, **20**, 4181.
163 C. Lin, X. Zhu, J. Feng, C. Wu, S. Hu, J. Peng, Y. Guo, L. Peng, J. Zhao, J. Huang, J. Yang and Y. Xie, *J. Am. Chem. Soc.*, 2013, **135**, 5144.
164 S. Jeong, D. Yoo, J.-t. Jang, M. Kim and J. Cheon, *J. Am. Chem. Soc.*, 2012, **134**, 18233.